# SPECTRAL RESPONSES OF a-Si:H THIN FILM COLOUR SENSORS AND FOURIER TRANSFORM SPECTROMETER

by

Mekbib Alemu

A Thesis Submitted to
the School of Graduate Studies, AAU
in Partial Fulfilment of the Requirement
for the Degree of Masters of Science in Physics

ADDIS ABABA
June, 1997

# SPECTRAL RESPONSES OF a-Si:H THIN FILM COLOUR SENSORS AND FOURIER TRANSFORM SPECTROMETER

by

Mekbib Alemu

A Thesis Submitted to
the School of Graduate Studies, AAU
in Partial Fulfilment of the Requirement
for the Degree of Masters of Science in Physics

ADDIS ABABA
June, 1997

# ACKNOWLEDGEMENT

The experimental part of this work had been carried out in KFA-*Forschung-szentrum Jülich,* Germany. This was possible with the great help of Dr. Thomas Eickhoff who invited and allowed me to work in his research group. For this I am very much indebted to him and sincerely thank him. Thanks are also due to Mr. H. Stiebig who was supervising my work and was giving valuable comments and suggestions. I am happy to extend my thanks to Mr. D. Knipp without whom I was unable to succeed this much with colour sensors and the spectrometer.

Special thanks are due to Professor R.Y. Thakur, my advisor, for his consistent and unfailing advice, comments and encouragement.

To Ato Tesfu Kassaye who was helping me with computer related problems and W/t Gizework Zewdie who helped in printing this thesis, I am greatly indebted.

Finally, I would like to thank DAAD (*Deutscher Akademischer Austauschdienst*) for the financial support during my stay in Germany.

# Table of Content

# List of Figures

# Abstract

In characterising photovoltaic devices, one of the most important measurements is the spectral response measurement. Several information can be obtained from the absolute value of the spectral response at a given wavelength and from the shape of the spectral response curve. To get accurate information, precise methods of measurement of the spectral response is quite important. Fourier Transform Spectrometer is believed to be one of such measurement set up which furnishes us with accurately measured spectral response curves. The use of Fourier Transform Spectrometer (FTS) for measurement of spectral response is not a new application. It had been used to measure spectral response of both crystalline and amorphous silicon solar cells, even though the Differential Spectral Response (DSR) method is the most usual one. However, bias-voltage-controlled colour sensors are quite recent findings, and so far the spectral responses of them were obtained from the Differential Spectral Response measurement. Here, the use of Fourier Transform Spectrometer for measurement of spectral response of a-Si:H thin film colour sensors was studied by measuring the spectral response of selected colour sensors and some of the problems associated with this application were identified. Finally suggestions to improve the set up were given.

# 1. Introduction

Sensors with colour recognition abilities are required in many domestic, agricultural, medical, industrial, and office applications. The progress in manufacturing and information technology has started a rush for high performance and compact intelligent sensor systems with good colour recognition capability and superior photoelectric properties[1]. The traditional way of identifying the colour of visible light, such as colour in vidicon, is to use the three band pass filters to extract the three fundamental components (red, green, and blue) of the incident light[2,3,4]. Most modern techniques for acquiring colour images, however, still produce colour pictures and colour information that are perceptibly different from the original scene. A major reason for this is difficult selection and fabrication of transmission filter sets that are suitable for incorporation into good quality colour cameras and colour sensors[3].

There is a hope of resolving these problems of filters by manufacturing colour sensors which do not use band pass filters. Leaving out the filters has also the advantage of realising more compact intelligent sensors. Such a sensor with two component colour recognition ability was proposed about 10 years ago by H.K. Tsai, S.C. Lee, and W.L. Lin[5]. This was soon revised and improved to a standard RGB (Red, Green, Blue) sensor[6]. Since then, several improvements were made and the number of component colours detected had been improved[2].

The new type of colour sensor is based on hydrogenated amorphous silicon (a-Si:H) hetrojunction. The peak spectral response (the output photo current per unit incident photon flux) of the sensor is shifted from one wavelength to the other without using band pass filters. This is achieved only by changing the applied bias voltage to the device. Amorphous silicon was chosen for the construction of these devices due to its multi - advantageous characteristics. With AM-1 incident illumination the conductivity of a-Si:H typically changes by a factor of more than $10^5$ and hence provides low series resistance in a device configuration, which is an important feature for obtaining optimum conversion efficiency[7]. On top of this, amorphous silicon has more than one order of magnitude higher absorption coefficient compared to c-Si in the visible region[8]. Hydrogenated amorphous

silicon exhibits not only excellent photoconductivity and high absorption, but also it can be doped both n- and p-type[7]. Its moderate processing temperature of about 250°c allow the use of low-cost substrates such as glass[7,9]. It also offers the possibility of forming thin-film transistors for addressing circuits. The need for fast and compact intelligent sensor was suggested and demonstrated[2,10] to be met by combining a-Si:H sensors with the fast crystalline silicon red out circuitry. This compatibility of a-Si with c-Si and the possibility of using the c-Si technology to produce a-Si with suitable characteristics for device application make a-Si attractive.

Even if amorphous silicon has all the advantages listed above, it has some limitations. The most important of all being its photovoltaically unstable nature. This was first demonstrated by D.L. Staebler and C.R. Wronski[11]. The Staebler-Wronski effect describes that when amorphous silicon is exposed to light the defect density of the material increases leading to deterioration of its electronic properties. In spite of this fact, observations made with 1000Lux illuminations for about 64hours have indicated that the amorphous colour sensors depict no such degradation[12]. Taking into account the long exposure time, this illumination level is considered quite strong in comparison to practical application of the colour detectors, e.g., in video camera system.

The main important characteristics of a-Si:H thin film colour sensors (and even of any kind of colour sensor in general) are the linearity of the response of the device with respect to the input radiation, the colour separation ability, the dynamic range, and the transient behaviour of the device. In this work we concentrated our attention on the measurement of the spectral response of three kinds of a-Si:H colour sensors. The spectral response measurement gives information about the colour separation ability of the sensors. The aim of this work is to use Fourier Transform Spectrometer (FTS)[13] as a new set up for measuring spectral response of the devices. Using FTS to measure spectral responses of photovoltaic devices is not a new application. J. Beier, A. Schonecker, and A. Zastrow had used it for solar cell calibration[14]. They compared the results of spectral response measurements of FTS with other two techniques. K. Bucher and A. Schonecker[15] had also used it with somewhat similar set up as the one used in this work. The main difference in

our set up is that bias voltage is applied to the sensors and this causes a considerable dark current.

In the study of the colour separation ability of the a-Si:H thin film colour sensors, several spectral response curves are required. This in turn requires a great deal of time in the usual measurement set up using the Differential Spectral Response (DSR) method[16]. A conventional grating spectrometer such as DSR set up receives information from the very narrow range which is limited by the slit-width of the instrument, and hence, requires considerably large measurement time to cover the whole range of a spectrum. With a FTS it is possible to get information about the whole range of a given spectrum during each scan time element (about 0.2sec). This makes data collection with FTS a very fast process. Among other facts, this reduction of measurement time with FTS set up is the main temptation to any one interested in measuring spectral response of a-Si:H thin film colour sensors.

The basic idea of the measurement with FTS is based on comparing the spectra obtained by using two detectors: amorphous and crystalline silicon detectors. Since the spectral response of one of the detectors (c-Si detector) is known, the spectral response of the other (a-Si:H detector) is obtained. The basic assumption in this work is that the spectrum of the white light source is time independent. In this work, as the use of FTS for studying a-Si colour sensors was the first attempt, several improvements were made in the measurement set up in order to put it in a good measuring conditions. Care was also taken to minimise the influence of improper functioning of the sensors on the data obtained by using FTS. To this end, measurements of linearity and dynamic range were made and only those thin film colour sensors which showed reasonably good behaviour were chosen. Before using the samples in the FTS set up I-V measurements were also made for identifying the application range of the sensors.

In this paper the results of the spectral response measurements using FTS are compared with the data obtained from the DSR set up. Possible sources of differences between the two sets of measerement data are identified. Suggestion to reduce the effects of them in further study are presented.

# 2. Amorphous Silicon Thin Film Colour Sensors

## 2.1 Concepts of Colour Sensation

Light is electromagnetic radiation that is capable of producing visual sensation in human observer. Electromagnetic disturbance propagates through space as a wave. Such a wave can be considered as a superposition of purely sinusoidal waves each of a fixed frequency[17]. The distribution of energy among these components is called the spectrum of the radiation. Those parts falling into the range of about 0.38 to $0.78 \times 10^{15}$Hz (380 to 790nm) can cause visual sensation[18], therefore they are properly called light.

In a measurement involving light, if the total power within the visual range as well as those outside are included, the process of the measurement is called **radiometry**[18,19]. The adjective **radiant** is used to qualify radiometric quantities. When the power is included only to the extent that is visible, the process is called **photometry**[18,19], and the adjective **luminous** describes the quantities measured. **Colorimetry**[19] refers to the measurement of radiation in terms of their effectiveness in producing the sensation of colour.

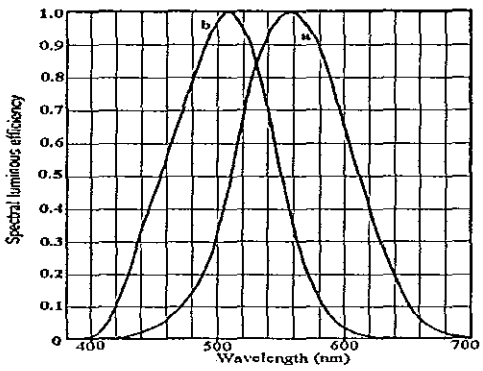


**Fig.2.1** The Visibility curves (a) for photopic; (b) for scotopic human eye. (adapted from Ref. 18).

It is found that to the photopic (light adapted)[19] eye, radiation near 555nm is most effective and that visibility drops on both sides of this wavelength, approaching zero at about 400nm and 700nm, respectively. When normalised relative to the maximum, the visibility at any wavelength $\lambda$ is referred to as the **spectral luminous efficiency** ($k_\lambda$). The exact course of visibility varies slightly from one observer to the other. It has, however, been standardised as shown in Fig.2.1.

Radiation with a given spectral distribution will produce, in a normal observer, a specific colour sensation. The converse, however, is not true: a given colour sensation can be produced by an infinite number of spectral distributions. Thus, despite its intimate connection with the radiation spectrum, colour has an existence

independent of this spectrum. This aspect of colour, which does not concern itself with spectral composition and works exclusively with sensation is referred as psychological[18]. The psychological treatment of colour is based on Grassmann's law[19]:

1. The eye can discern only three types of colour variations, expressible as hue, brightness, and saturation.
2. If, in a mixture of two unequal colours, the proportion is steadily changed, the colour of the mixture changes.
3. When lights of two given colours are mixed, the result is always the same, regardless of the particular spectral compositions that produce the two colours in the mixture.
4. When two lights are mixed, the luminous flux of the mixture equals the sum of the luminous fluxes of the components.

Grassmann's first law implies that colour is three dimensional and therefore may be represented in three-dimensional spatial coordinates. Such a representation is then called a colour solid. One possible set of dimensions has already been mentioned[18]:

1. Hue represents that aspect of colour whose change is implied as it varies from blue to green or from red to purple.
2. Saturation measures the purity of the colour; it decreases as grey is approached.
3. Brightness is a measure of the magnitude of the total sensation. Terms like luminance for self luminous object, lightness for surface colours, and clearness for transparent objects are used in specific cases for this third dimension.

The three coordinates can be plotted in cylindrical coordinates, the brightness being plotted along the vertical axis, the hue as the azimuth angle ($\theta$) and saturation as the radial distance from the axis. In this arrangement white is at the top of the axis, black at the bottom, and the neutral greys are arranged along the axis between them. Red is at $\theta=0$, green at $\theta=\pi$, blue at $\theta=\pi/2$, and yellow at $\theta=3\pi/2$. The purity of these colours increases with their distance from the axis (see Fig 2.2(a)). It is also possible

to represent the colour solid in terms of a rectangular coordinates (Fig2.2(b)). The location of colour in a plane normal to the lightness axis is called its **chromaticness**. It is two-dimensional and may be specified for instance, in terms of hue and saturation or redness and yellowness.

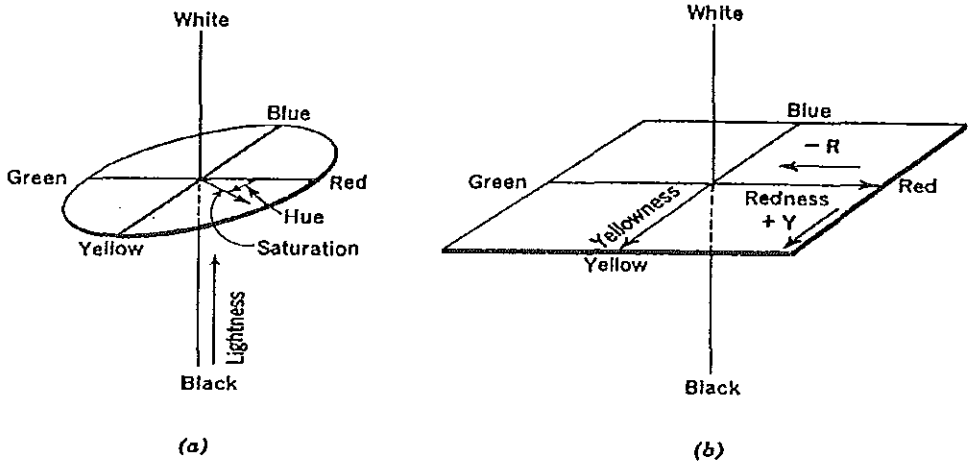


**Fig.2.2** The colour solid (a) cylindrical coordinat; (b) rectangular coordinates. (adapted from Ref.18)

When three light sources, differing in hue, are available, a continuous, three-dimensional gamut of colours can be generated by mixing them in various amounts. When these light sources are judiciously chosen, by far the major portion of all chromaticness values can be generated by this method, called **Tristimulus colorimetry**. The three colours chosen are called **primaries** and the amount of each required to generate a particular colour is the corresponding **tristimulus values**.

Our colour vision is based on the fact that it resolves a given colour stimulus into three components based upon three primaries (red, green, and blue)[18,19]. Colour is perceived in the retina of the eye by three sets of cones, these being receptors with maximum sensitivity to blue (430nm), green (530nm), and red (600nm) as shown in Fig. 2.3.[20]

To identify a colour stimulus the responses by the colour sensing cells in the eye to different wavelengths have been standardised and incorporated into the Commission International de l'Eclairage (CIE)[21] Standard Observers for Colorimetry. It is designed to be representative of a typical observer. The colour matching response functions x, y, z, of a CIE Standard Observer are shown in Fig. 2.4[22].

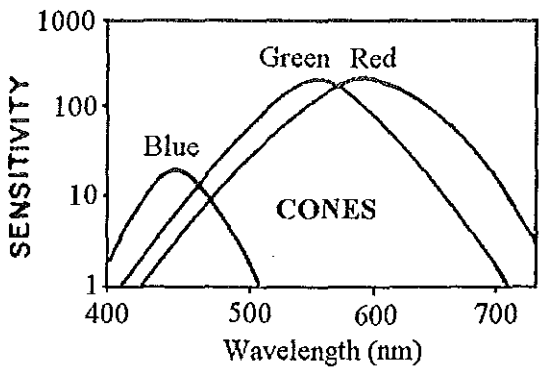


**Fig.2.3** Relative sensetivity of the CONES of the human eye[20].

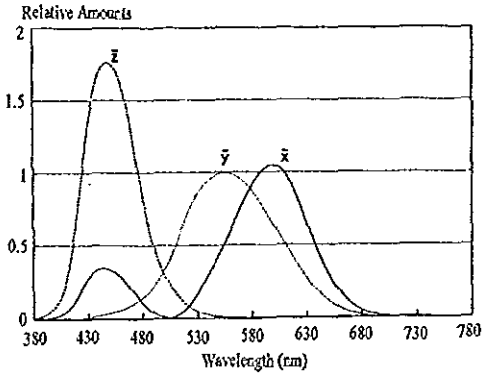


**Fig.2.4** CIE tristimulus values of equal energy spectrum[4].

Based on these colour matching functions, the tristimulus values X, Y and Z of any object can be obtained using[4]:

$$X = 100 \frac{\sum E_\lambda R_\lambda \bar{x}_\lambda \Delta\lambda}{\sum E_\lambda \bar{x}_\lambda \Delta\lambda} \qquad (2\text{-}1a)$$

$$Y = 100 \frac{\sum E_\lambda R_\lambda \bar{y}_\lambda \Delta\lambda}{\sum E_\lambda \bar{y}_\lambda \Delta\lambda} \qquad (2\text{-}1b)$$

$$Z = 100 \frac{\sum E_\lambda R_\lambda \bar{z}_\lambda \Delta\lambda}{\sum E_\lambda \bar{z}_\lambda \Delta\lambda} \qquad (2\text{-}1c)$$

where $E_\lambda$ is the energy of the white light source at wavelength $\lambda$ and $R_\lambda$ spectral reflectance of the object being observed. Knowing the tristimulus values, the colour of the object can be defined.

## 2.2 Working Mechanisms of Colour Sensors

In constructing colour sensors an attempt is made to imitate the operation of the human eye. So far, optical filters were integral parts of such colour sensors. Any colour is decomposed into three primaries using three filters and the tristimulus values are measured separately by an appropriate circuitry. One representative diagram of colour sensor used in colour scanning is shown in Fig.2.5. For colour recognition, in this arrangement, CCD (charge coupled device) sensors[3,22,23,] are used. Basically the same set up is used with optical fibber sensors[4]. The operation of the a-Si:H thin film colour sensors, however, need no colour filter. Instead of colour filters the sensitivity of the detector is adjusted by an externally applied bias voltage.

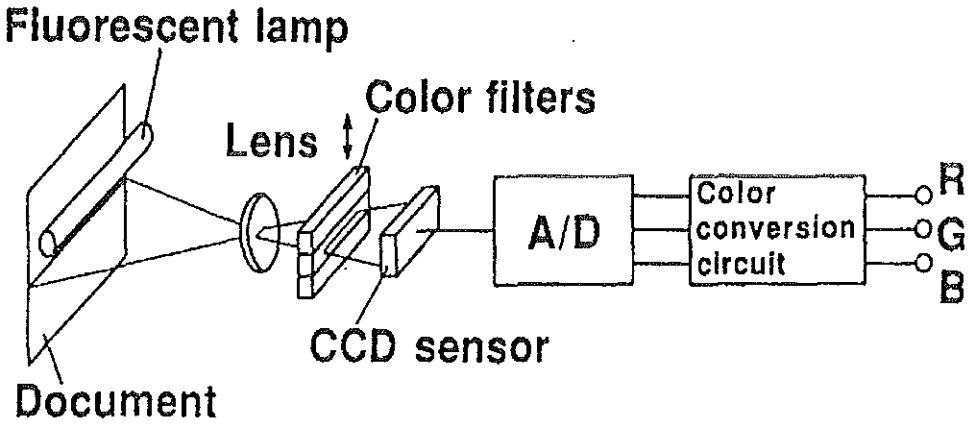


**Fig.2.5** Representative schematic diagram of colour scanner with colour filters [21].

To realise a semiconductor photodetector with colour recognition ability, photosensitive material is used. In general three basic processes take place in photosensitive devices[23]:

1. Carriers are generated by absorption of incident light,
2. Carriers are transported and/or multiplied by whatever current gain mechanism,
3. Interaction of current with the external circuit provides the output signal.

With proper modification in the first two processes, one can get different output signals to different incident light.

For the colour sensors studied in this work, the incident light was made to be absorbed in different parts of the active body of the sensors. This was done with the knowledge of frequency (wavelength) dependence of penetration depth of electromagnetic radiation in absorbing medium[24] and by sequencing materials of different band gap in suitable order.

When a semiconductor is illuminated with light, the photons may be absorbed or they may propagate through the semiconductor, depending on the photon energy hν and the energy gap $E_g$. If the photon energy is less than $E_g$, the photons are not readily absorbed and if hν is larger or equal to $E_g$ the photons will be absorbed and may produce electron - hole pairs in semiconductor. The portion of the absorbed photon flux is determined by absorption coefficient of the material and the distance

the photons travelled within the material. This can be seen from the exponential decay of the intensity of the photon flux with distance, given by the equation[25]

$$I_\nu(x) = I_{\nu_O} e^{-\alpha x} \qquad (2\text{-}2)$$

where $I_\nu$ is the intensity of the flux of photons of frequency $\nu$ at depth x, $\alpha$ is the absorption coefficient of the material which is dependent on frequency, and x is the distance within the material. For a-Si and c-Si the dependence of $\alpha$ on wavelength (frequency) is shown in Fig.2.6. From this figure one can easily see the superiority of a-Si over the crystalline one in absorption in the visible range.

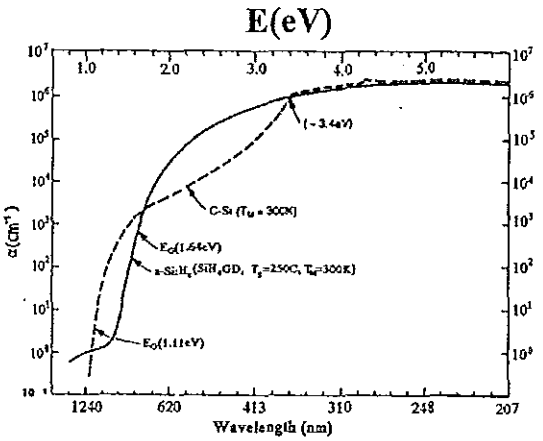


**Fig.2.6** The absorption curves of a-Si (solid) and c-Si (broken)[8].

The long wavelength cut-off for absorption of electromagnetic wave is determined by the band gap as given by[23]:

$$\lambda_c = \frac{hc}{E_g} = \frac{1.24}{E_g(eV)} \qquad (2\text{-}3)$$

So, as the energy gap gets larger and larger the cut off wavelength gets smaller and smaller. Hence, if two materials of different band gap put side by side, with the wider band gap material at the light entrance side, most of the photons of wavelength smaller than $\lambda_C$ will be absorbed in the first layer and part of the flux of photons having wavelength greater than $\lambda_C$ of the first layer will be transmitted into the second layer. The same happens to the transmitted flux and still those having wavelength larger than $\lambda_C$ of the second layer will be transmitted out. Therefore, if a third layer is put next to the second absorbing layer, part of the transmitted photons will have a chance to be absorbed. This means, effectively the incident light will be distributed according to its wavelength and different part of it will be absorbed in different parts of the absorbing semiconductor. This is one of the bases of operation of the thin film colour sensors used in this work.

Separate absorption of the incident light in different part of the photosensitive material does not guarantee differential output signals in the external circuit. The absorbed photon must produce electron-hole pairs and these electron-hole pairs

should be collected in the external circuit. If all the photogenerated charge carriers from different parts of the absorbing material are collected in the external circuit, no colour information is obtained. To get the colour information a means to separately collect the photogenerated carriers must be sought. This is made effective in the case of a-Si:H colour sensors by operating the above discussed stack in a photodiode mode[9,25] with the carrier collection region chosen by an applied bias voltage.

A photodiode is operated in reveres bias conditions. In reverse bias the photodiode has a depleted semiconductor region with a high electric field that serves to separate photogenerated electron-hole pairs. The width of the depleted region depends on the magnitude of the reverse bias voltage $V_R$, as given by[26]:

$$W \approx \left\{ \frac{2\varepsilon_s [V_{bi} + V_R]}{eN_B} \right\}^{1/2} \qquad (2\text{-}4)$$

where $V_{bi}$ is the built-in potential between the doped and undoped region of the photodiode, $N_B$ is the concentration of doping, and $\varepsilon_s$ is the permittivity of the material. W in the above equation gives the width of the depleted region in the photosensitive part of the photodiode which is usually undoped. Thus, by properly choosing the reverse bias voltage and consequently the width of the depleted region, one can determine from which part of the stack carriers will be collected.

This partial separation may not, in actual application lead to separately obtaining the differential signals corresponding to different stimuli. Another way of separately collecting the photogenerated charge carriers is by properly ordering the photosensitive layers according to the life time $\tau$ of carriers in the materials. The life times of electrons and holes are generally controlled by recombination centres and traps present in the forbidden gap of the photosensitive material[27].

The photocurrent obtainable for a given illumination level is affected by the life time of the photogenrated carriers. In a material where the transit time $t_T$ is longer than the life time $\tau$, the photogenerated carriers will recombine effectively before reaching the boundaries of the material. Thus, these carriers will not contribute to the output signal in the external circuit. Therefore, even if electron-hole pairs are generated in two parts of a reverse biased photodiode simultaneously, there is a

chance of collecting carriers from only one part while those in the other part recombined due to short life time compared to the required transit time.

The transit time is given by[9,26]:

$$t_T = L/v_d = L/\mu E = L^2/\mu V \qquad (2\text{-}5)$$

where $v_d$ is the drift velocity, $\mu$ is the free-carrier mobility, E is the electric field, V is the applied voltage, and L is the length of the material. The photocurrent contribution of that part of the depleted region in the steady state is given by[27]:

$$I_{ph} = qFG \qquad (2\text{-}6)$$

where q is the electron charge, F is the total number of free charge carriers generated per second in the photosensitive material under illumination, and $G=\tau/t_T$ is the photoconductive gain. Hence, rewriting the current in terms of external parameters we have[27],

$$I_{ph} = q\frac{F\mu\tau}{L^2}V \qquad (2\text{-}7)$$

From this result one can see that it is possible to adjust the contribution of the photocurrent from a given layer of a given $\mu\tau$-product and length L by adjusting the applied voltage.

The discussion so far demonstrated that it is possible to absorb the incident photon flux in different layers according to their location in the energy (or wavelength) spectrum. Further, two ways of separately collecting carriers from different parts of the stack of photosensitive material were discussed. The former was possible by proper band gap structuring while the latter was accomplished by controlling the bias voltage and the $\mu\tau$-product structuring of the layer stack. Applying these concepts different a-Si:H thin film colour sensors were designed[2,5,6,28]. The three basic once are described below.

## 2.3 Different a-Si:H Thin Film Colour Sensors

### 2.3.1 The n-i-p-i-n Three Colour Detector

The first a-Si:H hetrojenction reported in 1987 by H.K. Tsai, S.C. Lee and W.L. Lin[5] was a two colour sensor. It was the first colour sensor operating without colour filters reported. Since then several improvements as to the quality of the colour separation and the number of colours detected were made. The maximum bias voltage needed was also reduced from about 10V to about 3V. The first improvement made was the construction of a three colour sensor whose operating voltage was about 2 volts[6]. The recently optimised three - colour detector was reported to have good colour separation[29]. The basic factors that should be considered in optimising the device property will be discussed in the following section of this chapter. Here the three colour sensors are discussed in general terms.

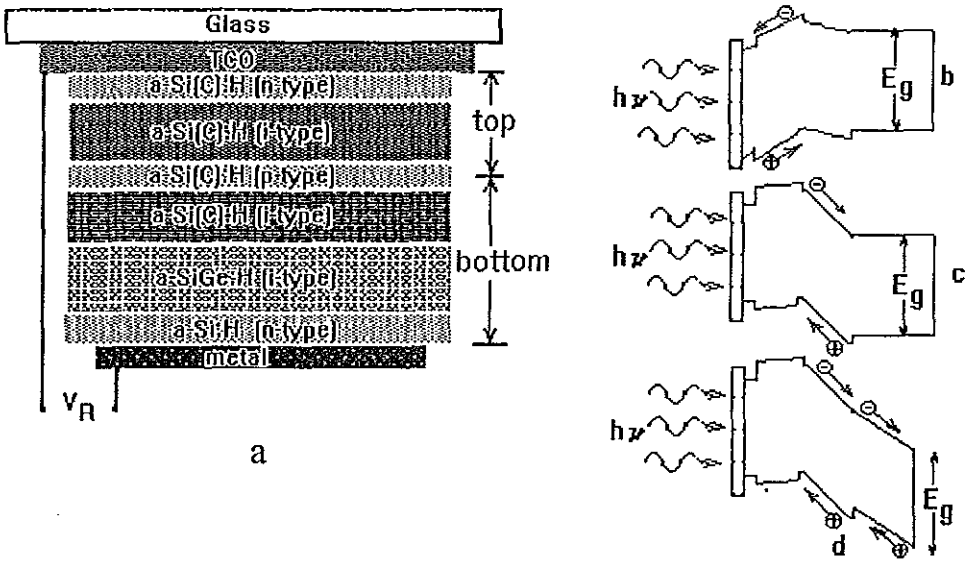


**Fig. 2.7**a) Schematic cross section of a n-i-p-i-n three colour detector. The bandgap diagram shows the detector: b) under positive bias, c) under small negative bias, d) under larg negative bias.

Our discussion of three colour sensors will be concentrated on n-i-p-i-n structures because for this layer sequence electrons dominate the carrier transport, in contrast to p-i-n-i-p sensors[25,30]. This structure consists of two back-to-back p-i-n junction diodes (see Fig. 2.7). The diode on the illuminated side (henceforth the "top diode") consists of a wide band gap a-Si(C):H. The wide band gap a-Si(C):H has three parts two of which are highly doped regions

and the region between the two is completely undoped i-layer. The photovoltaically active region is this i-layer. The diode on the rear side (henceforth the "bottom diode") consists of a-Si(C):H p-layer, a-Si(C):H i-layer, a-Si(Ge):H i-layer, and a-Si:H n-layer. The whole of the layer stack is covered by a Transparent Conducting Oxide (TCO) and glass substrate at the light entrance side and with aluminium rear contact at the back side.

The Difference in the band gaps of different layers and the wavelength dependent absorption coefficient render the incoming photons to be absorbed in different layers. The high energy photons are mainly absorbed in the top diode, whereas low energy photons are absorbed in the bottom diode. Taking absorption coefficient and thickness into account the amounts of absorbed photons in different layers could be determined[30]. For a given layer stack used in Ref. 19 it has been determined from optical transmission measurements, that more than 90% of the blue light (450nm), approximately 35% of the green light (500nm) and only 5% of the red light (650nm) is absorbed in the top diode. The remaining blue light, the remaining green photons and approximately 55% of the red photons are absorbed in the bottom diode.

Changing the polarity of the applied bias voltage to the colour sensor one of the two back-to-back connected diodes can be selected to collect the photogenerated carriers. When a positive bias voltage is applied to the TCO with respect to the aluminium back contact the top diode is reverse biased and the electrons generated by blue photons will be collected. The blue generated holes will be trapped and recombined in the highly doped $P^+$ layer because this layer has high defect density and therefore acts as a recombination plane[31]. In the forward biased bottom diode, since the electric field is very weak the photogenerated electron-hole pairs will not be separated and thus will not contribute to the output current. On the other hand, when a negative bias voltage is applied the bottom diode is reverse biased and photogenerated electrons in this region by green and red photons will be collected. Which of the electrons will be collected depends on to which extent the depletion region is extended and/or on whether the transit time is less than or greater than the life

time $\tau$ of the layers. In this case too, the photogenerated holes will be recombined.

As discussed in the above paragraph, the device shows preferential responses to different wavelengths according to the applied bias. For n-i-p-i-n three colour detector peak responses to blue light for positive bias voltage, to green for small negative bias ($\approx$-1V), and to red for larger negative bias voltages were obtained. Therefore, just like the set of cones in the retina the detector can be used to distinguish colour by determining the tristimulus values of the primaries.

## 2.3.2 The n-i-p-i-n Multi-Spectral Colour Detector

The multi-spectral colour (The Five Colour) sensor[2] uses basically the same principles as a three colour sensor. Only two more additional i-layers in the top and bottom diodes of the three colour detector are introduced. Band gap and $\mu\tau$-product engineering in the top and bottom diode of the n-i-p-i-n three colour detector in order to improve the spectral separation of the device lead to additional peak responses. The band gap and $\mu\tau$-product structuring of the multi-spectral colour detector is shown in Fig. 2.8. For the optimised structure the band gap of each layer decreases from the front contact to the back contact, whereas the $\mu\tau$-product of the layers increases from the n-layer to the p-layer.

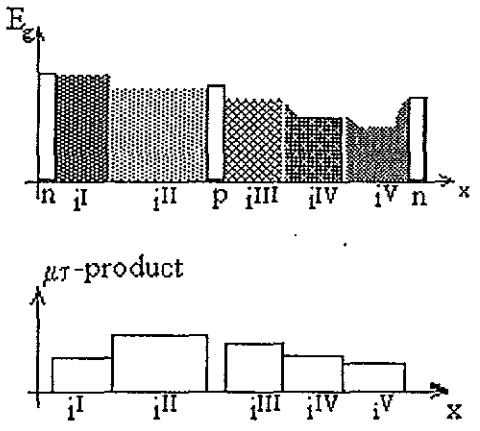


**Fig.2.8.** $E_g$ and $\mu\tau$-product stracturing of the multi-spectral colour detector[2].

Here too, photons of different wave wavelength will be absorbed in different layers. Selective collection of photogenerated carriers is also controlled by the applied voltage. For low positive voltages the top diode is reverse biased and carriers from region II are collected due to their larger life time in that layer. Caused by a low $\mu\tau$-product in region I the photogenerated carriers in this region recombine effectively.

Increasing the applied voltage will extend the collection region into the first i-layer and carriers in this region will be collected additionally. For the case of negative bias the bottom diode is reverse biased and depending on the magnitude of the voltage the collection region extends over the third, the third and the forth, or the entire bottom diode. Consequently, photogenerated carriers from the respective regions will be collected. In this device as well, the $p^+$ layer blocks the photogenerated holes from reaching the extrnal circuit.

## 2.3.3 The p-i-n Three Colour Detector

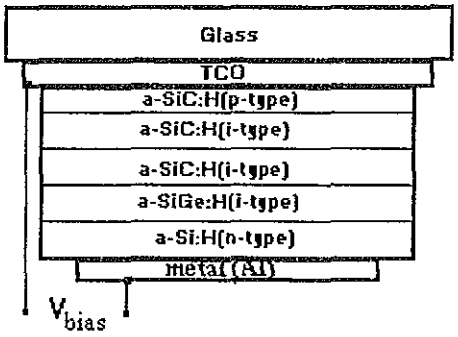


**Fig. 2.9** The p-i-n three colour detector. It is basically the same as the bottom diode of the five colour detector.

The p-i-n three colour detector[28] is the direct consequence of the possibility of obtaining three distinct signals from the bottom diode of the multi-spectral colour sensor. The structure of this detector is similar to the bottom diode of the latter as shown in Fig.2.9. A stack of three i-layers differing in band gap and $\mu\tau$-product were sandwiched between the front p-layer and the back n-layer. One can also think of this structure as a single p-i-n solar cell. Except that only negative bias voltage is used to collect carriers the working mechanism of this detector is the same as described in the preceding two sections.

## 2.3.4 Preparation of a-Si:H Thin Film Colour Sensors

Most of the compositional and physical properties of hydrogenated amorphous silicon are determined by the growth method and processes. Even though there are numerous a-Si:H film deposition techniques[7,9] a Glow

Discharge or Plasma Enhanced Chemical Vapour Deposition (PECVD) technique is the most important and widely used one in preparing films for device applications. In this technique the major steps are source gas (silane $SiH_4$) diffusion at a controlled rate, electron impact dissociation and formation of the plasma, gas-phase chemical reaction, radical diffusion into and deposition on the substrate which is maintained at a strictly controlled temperature.

The electronic characteristic of the resulting film is determined by such parameters as substrate temperature, gas flow rate, pressure, concentration, power etc. PECVD method is found to be attractive due to its incorporation of the dangling bond terminator hydrogen in the film. In addition to passivating the dangling bonds and reducing the defect density, hydrogen increases the optical gap of the material[12]. The hydrogen content of the film is correlated with the substrate temperature. Thus, for example, the defect density and the optical gap of a-Si:H film can be controlled by controlling the substrate temperature.

In the colour sensor structure the illuminated side is made up of wide band gap material. The wide gap material is amorphous silicon carbide alloy. It is obtained using silane and methane as source gases. The carbon alloying results in an optical band gap of higher than 2eV[1]. In the rear part of the sensors, narrow band gap material, a-Si(Ge):H is used. This is obtained by using gas mixtures of silane, germane, and hydrogen.

The p- and n-type doped layers were realised by adding diboron or phosphene, respectively. However, the defect density and the optical band gaps are not independent of the doping concentration. While the defect density increases with the square root of the doping concentration[29] the band gap for p-type a-Si:H decreases with increasing doping level. For a beneficial enhancement of the defect density of the p-layers high doping is used[31]. It worths noting that the defect density and the band gap are also affected by the carbon and germanium contents.

## 2.4 Important Factors To Realise Optimised Colour Sensors

The fundamentals of operation of colour sensors being as described in the previous section, the quality of their performance depends on several factors. A colour sensor that is capable of giving specific signals corresponding to more than three colours may not necessarily be good in its response speed or a sensor that has good colour separation and good response speed may not have a proportional response to different illumination levels. Furthermore, the different factors affecting the performance of a colour sensor are not independent of each other. Therefore, in realising a given colour sensor a balance should be struck between them. In this respect the main factors that need consideration are the linearity of the device, the colour separation ability, the dynamic range, and transient behaviour of the device.

### a) Linearity:

Linearity is defined as the property that the output quantity of the detector is proportional to the input quantity over a specified range. Similarly it may be defined as the property that the responsively of the detector is constant within a specified range [32].

Most radiometric or photometric measurements are ratio measurements. The detector is calibrated under a given condition. Then from the ratio of the response in an unknown condition to the response in the calibration condition or using the response in the calibration condition as a reference response, the required information about the unknown is determined. Every measurement with a radiometer, photometer, or colorimeter implies such a process.

A detector may be inherently linear but unsuitable electronics may make the detector-electronics combination non-linear. The typical example is combination of a linear silicon photodiode with an amplifier

or digital voltmeter of high input impedance. The combination has a logarithmic characteristics[32].

## b) Colour Separation:

The colour separation is the ability of the colour sensor to give distinct responses to different colour stimuli. The less the overlap between two response curves the better the ability of a detector to distinguish colour. In general, narrow spectral response curves are assumed to give good colour separation[33].

In the multi-layer structure a-Si:H thin film colour sensor, the p-layer has a major influence on device performance. For a n-i-p-i-n structure with high defect density ($N_{db,p}$=$10^{19}cm^{-3}$) in the p-layer spectral separation for red and blue was observed to be better than for the one with lower defect density ($N_{db,p}$=$10^{17}cm^{-3}$) in the p-layer[31]. Additional defect layers on both sides of the central p-layer were observed to improve spectral separation[12,31].

## c) Dynamic Range:

The performance of an optoelectronic device is determined by the ratio of the photocurrent to dark current which will be referred to as the dynamic range D. It is strictly defined in terms of the photocurrent at an illumination level of 1000Lux from halogen lamp according to

$$D(dB) = 20\log\frac{j_{1000lx}}{j_{dark}} \qquad (2\text{-}8)$$

It was defined in terms of the photocurrent at 1000Lux because no saturation has been observed for a-Si:H detectors under realistic conditions[2].

The dynamic range of a-Si:H colour sensors is mainly determined by the dark current. Near zero bias voltage the dynamic range had large values due to insignificant dark current for small voltages. At higher bias voltages the dark current will increase considerably and the dynamic range consequently decreases. A value of 90dB is assumed to be appropriate for signal processing[30].

## d) Transient Behaviour:

The idea of colour recognition with a-Si:H thin film sensors is based on sequentially addressing each sensor element with different optimised photosensitive bias voltages. Thus, for continuos operation, different bias signals need to be successively applied to the sensor. This might cause a distortion of the signal due to charging or discharging effects of the deplition capacitance of the two diodes (in n-i-p-i-n structure). For low frequencies (about 10Hz) it was found that the response of the sensors is fast enough to follow the applied voltages[30]. However, for higher frequencies there is some distortion of the signal.

In order to improve the transient performance and to satisfy the frame rate conditions of standard Red-Green-Blue (RGB) signals, optimised colour sensitive voltages and optimised switching sequences have to be established. Different studies were made in this respect[1,2,28-30]. One of the results is that decreasing the positive bias voltage and increasing the negative bias voltage was found to minimise rise time of the photocurrent for n-i-p-i-n structure and switching from a particular blue sensitive voltage to green sensitive and then to red sensitive was considered suitable[29]. It should, however, need mentioning that high negative voltages can not be good solutions to reduce the photocurrent rise time because it results in a poor dynamic range.

# 3. The DSR And Fourier Spectroscopy

## 3.1 The Differential Spectral Responsivity Method

In characterisation solar cells the measurement of the spectral response is one of the basic steps[16]. The differential spectral responsivity (DSR) method is one of the measuring technique of spectral response. This method is also used to study the spectral response of other optoelectronic devices like colour sensors. The DSR method is spectroradionetric calibration procedure[16]. The measured quantity is the differential spectral responsivity $\tilde{S}(\lambda, I_{sc})$. It is a function of wavelength $\lambda$ and it is determined in the presence of steady-state solar like bias irradiance $E_b$ on the sample. This irradiance sets the operating point which is determined by the generated dc short circuit current $I_{sc}$ ($E_b$). Hence, the differential spectral responsivity is defined as[34]:

$$\tilde{S}(\lambda, I_{sc}) = \left.\frac{\Delta I_{sc}}{A \cdot \Delta E_\lambda}\right|_{I_{sc}(E_b)} \tag{3-1}$$

where A is the cell area, $\Delta E(\lambda)$ is the modulated quasi-monochromatic irradiance, and $\Delta I_{sc}$ is the generated short-circuit current. As this method was first meant for characterisation of solar cells[16] the operating points which are determined unequivocally by the dc short circuit current are given high emphasis. The dc short circuit current is photogenerated by the steady-state bias irradiance. The magnitude of $E_b$ as well as its spectral distribution determine $\tilde{S}(\lambda, I_{sc})$[16].

Steady-state bias radiation irradiating the test sample TS is produced by lamp BL (see Fig. 3.1). For solar cell case, the lamp BL usually used is a quartz-halogen tungsten lamp with a short pass filter (e.g. water filter) to get a sufficiently solar like bias irradiance. A solar like bias irradiance is needed because solar cell calibration must be made under a so called Standard Test Conditions[16]. Such a requirement is not, however, applicable for colour sensors for the time being. For suitable use of lock-in technique, the measuring radiation is chopped and passes through a monochromator MON, a shutter S and a beam splitter BS. To eliminate eventual offset effects, the result of measurement at each wavelength is taken as the

difference between the values measured with the shutter open and closed. The beam splitter is used to divert a definite part (about 7%) of the monochromatic

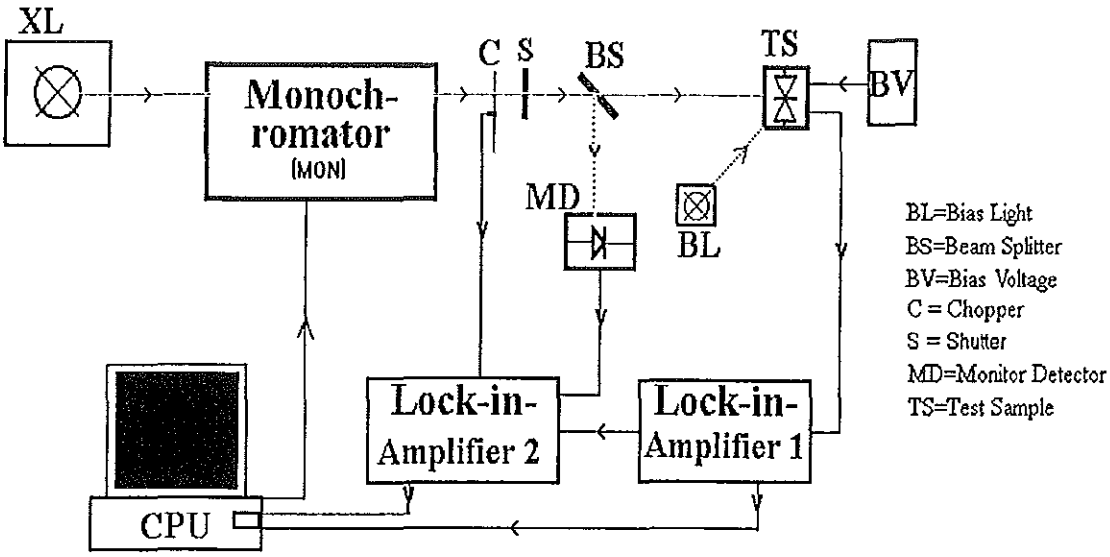


**Fig. 3.1** Block diagram of DSR apparatus. In this work the bias light was not used.

radiation onto the monitor detector MD. The ac short circuit current of the test sample and the monitor detector are measured simultaneously using two identical lock-in amplifiers. Any long-term and short-term instabilities of the lamp L will have no effect on the result of the measurement[34].

The output voltages of the lock-in amplifiers, the dc short-circuit current of the solar cell and the signals of various temperature sensors (not shown here) are stored and processed by the computer. The computer also controls the wavelength drive of the monochromator, the shutter, the currents of the bias lamps, and temperature of the sample. Thus, a fully automatic operation of the apparatus has been achieved. This full automation is one of the merits of the DSR apparatus over the Fourier Transform Spectrometer used in this work. However its time consumption in operation and the space it occupies made it inferior compared with the FTS set up.

The suitability of the DSR method for solar cell calibration[16] with large area[14] or with multi-layers[35] had been demonstrated elsewhere. As this method is well suited to study multi-layer structures, it has also been in use to measure spectral response of the a-Si:H thin film colour sensors. Unlike solar cells, colour

sensors are used in reality under a variety of illumination conditions including the solar like spectrum. Thus, it is not necessary to use a strictly solar like bias light in the DSR technique for the case of colour sensors. Some researchers, however use monochromatic bias radiation[6]. In this work no bias light had been used and therefore, instead of DSR, the abbreviation SR (Spectral Responsivity) was used simply to indicate that there is slight difference in application of the method here.

## 3.2. Fourier Transform Spectrometry

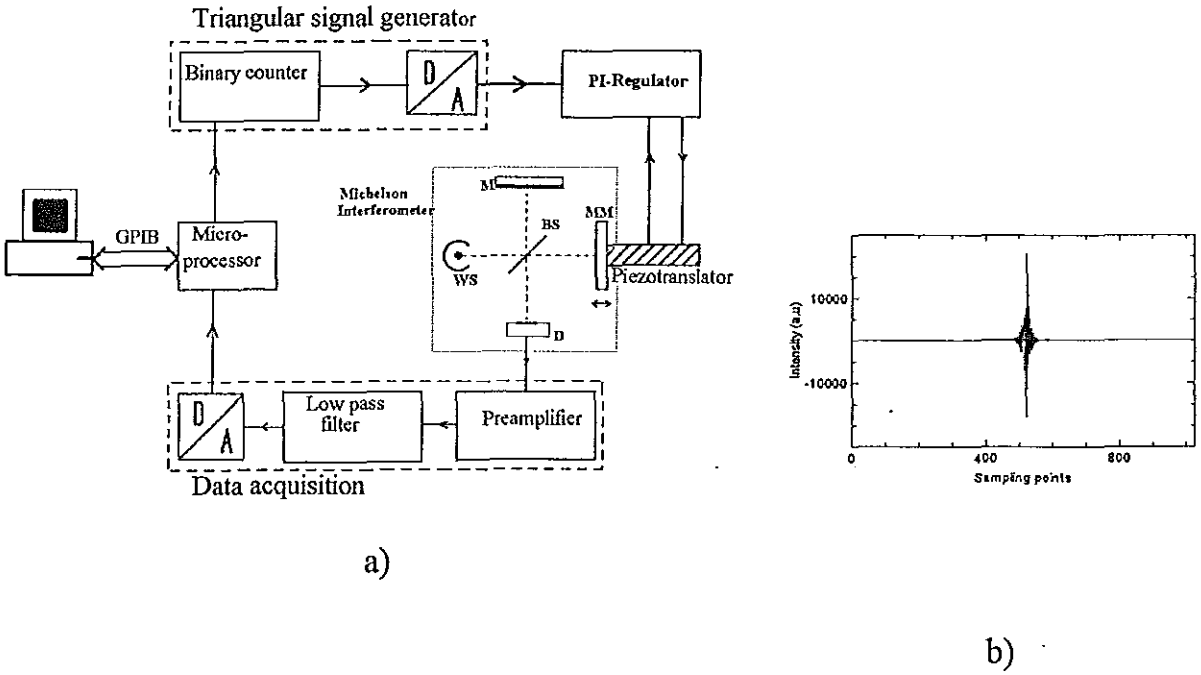


**Fig.3.2.** a) The block diagram of the Fourier Transform Spectrometer measurement set up. WS=White light Source, BS=Beam Splitter, MM=Movable Mirror, M=fixed Mirror, D=Detector. (Adapted from Ref.36)
b) A typical interferogram obtained with FTS. The interferogram is sampled at 1024 points.

The above diagram shows the set up of Fourier Transform Spectrometer (FTS)[13,36] used in this work to measure the spectral response of thin film colour sensors. The Michelson interferometer is the optical device which plays the central role in FTS. The upper part of the diagram shows the devices controlling the movement of the mirror MM attached to the piezo translator. This is done by

applying a triangular voltage to the piezo translator in discrete steps and monitoring the resulting movement using the feed-back obtained from the piezo translator. By applying a strictly controlled voltage to the piezo crystal set it is possible to move the mirror attached to it in precise steps. On the data acquisition side the signal detected by the detector will be amplified, digitised, processed, and finally stored.

In the interferometer, the light from the source (WS) is directed to a device called the beam splitter (BS). The beam splitter ideally allows half of the light to pass through while it reflects the other half. The reflected part of the beam travels to the fixed mirror M through a distance L. Then it is reflected there and hits the beam splitter again after a total path length of 2L. The same happens to the transmitted part of the beam. However, as the reflecting mirror MM for this arm of the interferometer is not fixed at the same position L but can be moved very precisely back and forth by a distance x about L, the total path length of this beam is accordingly $2*(L+x)$. Thus when the two halves recombine again on the beam splitter, they exhibit a path length deference or optical retardation of 2x. Since the two partial beams are spatially coherent they will interfere constructively when $2x=n*\lambda$ for n=0, 1, 2,... and destructively for 2x is an odd multiple of $\frac{1}{2}\lambda$.

Each wavelength in Michelson interferometer produces its own characteristic interference pattern as the movable mirror is displaced. A monochromatic source yields a cosine variation in the flux of the combined beams at the detector[37]. The period of the cosine function is uniquely determined by the wavelength and optical path difference for the radiation beams in the two arms. Each wavenumber band has its own characteristic cosine flux pattern with a particular magnitude at a given point (say at the centre of the interference pattern). The recording of the detected signal versus optical path difference is the interferogram (See Fig.3.2,b). For a source of many frequencies, the interferogram is the sum of the fluxes of each wavelength pattern. Fourier analysis enables one to convert the interferogram into a spectrum, i.e.; signal versus frequency. That is, Fourier analysis of the interferogram picks out the pattern for each frequency and determines the magnitude of the flux at that frequency, the Fourier coefficients.

The electric field part of a monochromatic light may be represented by[13]:

$$y(z,\sigma) = a(\sigma)\cos(kz) = a(\sigma)\cos(2\pi\sigma z) \tag{3-2}$$

where k is the propagation constant and σ is the wave number. If there are many waves of different wavelengths with amplitude a(σ), at a point, then the resultant amplitude at the point is

$$y(z) = \left(\frac{1}{\overline{\sigma}}\right)\int_0^\infty a(\sigma)\cos(2\pi\sigma z)d\sigma \tag{3-3}$$

where $\overline{\sigma}$ is some average wave number. Mathematically, it is convenient to work with exponential function than the cosine function, thus, the above equation can be rewritten as

$$y(z) = \frac{1}{2\overline{\sigma}}\int_{-\infty}^{\infty} a(\sigma)e^{i2\pi\sigma z}d\sigma \tag{3-4}$$

Defining $\frac{a(\sigma)}{2\overline{\sigma}} \equiv E(\sigma) \equiv$ the complex amplitude of the electric field at the wave number σ, one can rewrite the last equation as

$$y(z) = \int_{-\infty}^{\infty} E(\sigma)e^{i2\pi\sigma z}d\sigma \tag{3-5}$$

This equation gives us the amplitude of the resultant electric field as a function of position in terms of the Fourier transform of the electric field as a function of frequency[13].

The above result can be inverted and one gets

$$E(\sigma) = \int_{-\infty}^{\infty} y(z)e^{-i2\pi\sigma z}dz \tag{3-6}$$

where the electric field as a function of wavenumber is given as Fourier transform of the electric field as a function of position.

If we now consider two coherent waves, as in interferometer, which have the same amplitude $E(\sigma)$ at wave number σ, and which are separated by a phase difference 2πσδ at a given point, then the resultant amplitude at that point is

$$y(z) = y_1(z) + y_2(z) = \int_{-\infty}^{\infty}\left[E(\sigma)\left(1 + e^{-i2\pi\delta\sigma}\right)e^{i2\pi\sigma z}\right]d\sigma \tag{3-7}$$

If we define the resultant field as

$$E(\delta,\sigma) = E(\sigma)\left(1 + e^{-i2\pi\sigma\delta}\right), \tag{3-8}$$

then eq.(3-7) can be written as

$$y(z) = \int_{-\infty}^{\infty} E(\delta,\sigma)e^{i2\pi\sigma z}d\sigma \tag{3-9}$$

But the intensity B(δ,σ) (irradiance of flux density) is[18]:

$$B(\sigma,\delta) = \tfrac{1}{2}c\varepsilon_o E_R^*(\sigma,\delta)E_R(\sigma,\delta) \tag{3-10}$$

where $\varepsilon_o$ is the permittivity of free space and c is speed of light in vacuum. Substituting for $E_R(\delta,\sigma)$ from eq.(3-8) into eq.(3-10) we get

$$B(\delta,\sigma) = c\varepsilon_o E^2(\sigma)[1+\cos(2\pi\delta\sigma)] \tag{3-11}$$

Since there is no phase relation between the fluxes of different wave numbers at a given path difference δ from a white light source[13], we add the fluxes of different frequencies and define $I_R(\delta)$as

$$I_R(\delta) = \frac{1}{\overline{\sigma}}\int_0^{\infty} B(\delta,\sigma)d\sigma \tag{3-12}$$

Substituting for B(δ,σ) from eq.(2-11) and evaluating the integral at δ=0, one has

$$\left[I_R(\delta) - \tfrac{1}{2}I_R(0)\right] = \int_0^{\infty}\frac{c\varepsilon_o}{\overline{\sigma}}E^2\cos(2\pi\sigma\delta)d\sigma \tag{3-13}$$

It is usual to call $[I_R(\delta) - \tfrac{1}{2}I_R(0)]$ the interferogram even if $I_R(\delta)$ is sometimes called the interferogram. Writing the Fourier transform of this interferogram we have

$$\left(\frac{c\varepsilon_0}{\overline{\sigma}}\right)E^2(\sigma) = \int_0^{\infty}\left\{[I_R(\delta) - \tfrac{1}{2}I_R(0)]\cos(2\pi\sigma\delta)\right\}d\delta \tag{3-14}$$

Using the definition expressed in eq.(3-10) we obtain the basic equation of all of Fourier transform spectroscopy[13]:

$$B(\sigma) = (constant)\int\left\{[I_R(\delta) - \tfrac{1}{2}I_R(0)]\cos(2\pi\sigma\delta)\right\}d\delta \tag{3-15}$$

This equation states that if the flux versus optical path $I_R(\delta)$ is known, the Fourier cosine transform of $[I_R(\delta) - \tfrac{1}{2}I_R(0)]$ yields $B(\sigma)$, the flux density at the wave number σ. In order to obtain the spectrum, it is only necessary to repeat the calculation of the Fourier transform using eq.(2-15) for each wavenumber in the range of interest.

Note that, eq. (2-15) involves quantities defined within arbitrary multiplying factor since the electric field amplitude was defined in terms of a constant $\overline{\sigma}$ in eq.(2-4). This makes FTS to be applied only in measurements involving relative quantities[13,14,15]. To use this equipment for absolute spectral response measurements one needs a reference cell of exactly the same size as the test sample, or the test sample must fit completely into the central fringe[14]. The first option is impossible in colour sensor case as there is no standard reference detector.

In Fourier transform spectroscopy, the data actually obtained is the digitised version[38] of the interferogram. This is because the interferogram is sampled at N equally spaced points as the mirror is moved in discrete steps[13,36,38]. The Fourier transformation of this data thus requires the use of the discrete version of the Fourier transformation[38], i.e.,

$$B(k \cdot \Delta\sigma) = \sum_{n=0}^{N-1} I(n\Delta\delta)\exp(i2\pi n\, k/n) \qquad (3\text{-}16)$$

Where the continuos variables $\delta$ and $\sigma$ have been replaced by $n\Delta\delta$ and $k\Delta\sigma$, respectively. The spacing $\Delta\sigma$ in the spectrum is related to $\Delta\delta$ by

$$\Delta\sigma = \frac{1}{N \cdot \Delta\delta} \qquad (3\text{-}17)$$

In general case of measured data, the discrete Fourier transform must be calculated numerically by a computer though, it is possible to look up from an integral tables[38,39]. In practise eq.(2-16) is seldom used directly because it is computer time consuming. Instead a number of so-called Fast Fourier Transforms (FFT's) are in use. The most commonly used FFT is the Cooley-Tukey algorithm. The price paid for the speed is that the number of interferogram sampling points N can not be chosen at will, but depends on the algorithm[38]. For instance, the algorithm used in this work is Cooly-Tukey algorithm and the number of sampling points were 512 or 1024.

In the DSR method described in the preceding section, to construct the spectral response curves several measurements at different wavelengths are needed. On top of this, the study of the colour recognition behaviour of the colour sensors is based on obtaining several spectral response curves at different bias voltages. This process, is then definitely a time consuming one. In FTS this time consumption

could be reduced since in this method information about the entire range of the spectrum is obtained during one scan time. Furthermore, the acquisition of data at one time from the whole of the spectrum range gives the chance of obtaining information with the same background illumination from different sampling points of the spectrum (say 512 points).

# 4. Experimental Procedure

## 4.1 Current-Voltage Measurement

The spectral response measurement of the a-Si:H thin film colour sensors with FTS was the first attempt made to use the apparatus for this purpose. In order to see whether the data obtained with the measurement set up is reliable the a-Si:H thin film colour sensors used should have reasonable behaviour. Current-Voltage (I-V) measurements give sufficient amount of data for this purpose. From the I-V measurement data it is possible to get the dynamic range and to see the linearity of the device. It is also possible to get some information about the colour separation.

### 4.1.1. I-V Measurement Under Illumination.

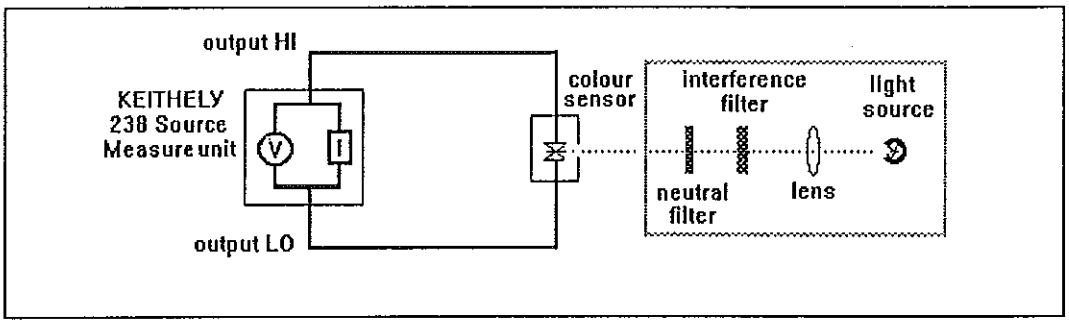


**Fig.4.1** The current-voltage measurement set up when the colour sensor is illuminated with light. For dark I-V measurement the sensor is put in a box and the part in the doted rectangle will not be included.

The set up shown in Fig.4.1 is the one used in this work for I-V measurement (both under illumination and without illumination). In the I-V measurement a computer controlled KEITHELY 238 High Current Source Measuring Unit was used. The measuring unit serves as a power supply to the sample and also it measures the resulting current. It is capable of measuring current down to $10^{-15}$ amperes range. The program used to run the measurement was a program written in HTBasic.

The first measurement taken under illumination was to see if the samples have colour separating ability. The sensors were illuminated with five different monochromatic light ranging from 450nm to 650nm. The illumination intensity for

all cases was $10^{15}$ photons/cm$^2$/sec. To get monochromatic light the incident beam from a halogen lamp was passed through interference filters with band width of about 20nm at different wavelengths. To get $10^{15}$photons/cm$^2$/sec level of illumination different predetermined amounts of current were supplied to the lamp. With this illumination on the sample, the photo current was measured varying the bias voltage starting from zero either to the positive or to the negative maximum value. The bias voltage was varied in discrete steps of 0.05V with a rest time of 3seconds between each step. This is to allow the current to reach a steady state.

The other I-V measurement was taken to check if the response of the samples are linear. In this measurement the set up shown in Fig.4.1 was used. The photocurrent was measured varying the monochromatic illumination from $10^{15}$photons/cm$^2$/sec to $10^{14}$ and $10^{13}$photons/cm$^2$/sec using neutral filters of transmittance of 0.10 and 0.01, respectively.

The third I-V measurement was done with 1000Lux illumination. This provides one of the input data to determine the dynamic range. To set the illumination level at 1000Lux a Luxometer was put exactly at the site of the sample and the current to the white light source was adjusted until the meter reads 1000Lux. Then the sample was replaced and the resulting photocurrent was measured. Here no filter was used.

### 4.1.2. The Dark I-V Measurement.

To measure the dark current (current under zero light illumination on the sample) the colour detector sample was put in a metal box which has special connecting terminal between the sample and the external circuit. This was to avoid light illumination on the sample and also to shield it from the ambient fields. Further to avoid the defuse light illumination of the sample the box was covered with black close. As described in section 4.1.1 the voltage applied to the sample was varied in discrete stapes to either positive maximum or negative maximum voltage starting from zero.

When the applied voltage was varied from positive to negative or vice versa without a pause at zero, the minimum value was found to be shifted to either side of

zero, and at zero bias an absolutely high current than the minimum was obtained. The figure below shows such an I-V curve. This was due to the discharging of the trapped charges from the previously reveres biased diode of the colour sensor as the biasing polarity was changed[34]. For this reason a dischrage time of about 15 minutes was allowed between the measurements in the positive and negative voltage sides.

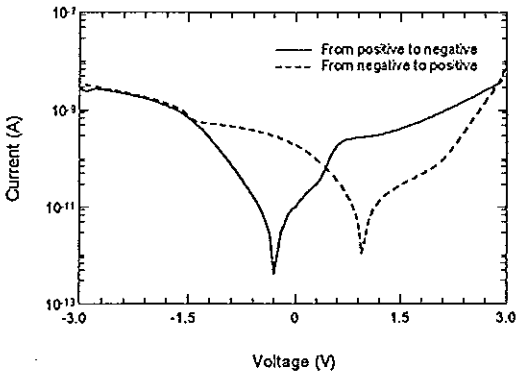


**Fig. 4.2** Current-Voltage curves measured without allowing a discharge time at zero Volt.

## 4.2 Measurement of the Spectral Response

### 4.2.1 Fourier Transform Spectrometer

To measure the spectral response of the a-Si:H colour sensors with the FTS, the set up shown in Fig.3.2 was used. To align the two mirrors of the interferometer and put them at equal arm lengths a HeNe-laser and mercury lamp were used. After that, when a tungsten halogen lamp (the white light source) was used and the interference pattern of the two beams from mirrors M and MM was focused on a crystalline PIN detector, an interferogram was obtained and seen on the monitor screen of the computer. The interferogram was seen on the screen with a background co-ordinate plane, with the horizontal axis representing the path difference and the vertical axis representing the intensity. Usually this interferogram was displaced to one side from the centre of the plane along the horizontal axis. Using the micrometer attached to the movable mirror holder the mirror was carefully moved to bring the centre of the interferogram at the centre of the plane. That is, as the horizontal axis represents the path difference between the two beams, a central peak of the interferogram centred at the centre of the plane corresponds to the one with no path difference. This last adjustment may result in

tilting of the mirrors with respect to each other. That was corrected using the mercury lamp.

When the mirrors were set exactly perpendicular to each other and the interferogram was at the centre, calibration of the set up with HeNe-laser was made. With this calibration the maximum wavenumber $N_{max}$ will be fixed and entire range will be divided into equal intervals. The maximum value $N_{max}$ will be used in transforming the obtained spectrum as a function of sampling points to a function of wavelength in nano-meters (nm). The transformation equation is

$$X = \left(\frac{512}{N_{max} \cdot x}\right) 10^7 nm \qquad (4\text{-}1)$$

How precise the calibration was carried out had been checked by measuring the intensity peak of the HeNe-laser. It must always be at approximately the same particular point, 633nm. This was done for every new set of measurements to ensure the precise arrangement of the interferometer.

After calibration, the HeNe laser was replaced by the white light source (halogen lamp) and the spectrum of the light was measured with the crystalline detector. At this point it must be noticed that the spectral distribution of the light from the halogen lamp is highly inhomogeneous as can be seen from the Fig. 4.3. The blue part has very week

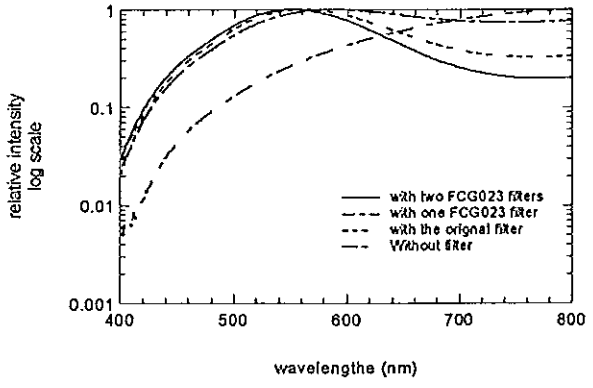


**Fig.4.3** White light spectra with different modifying filters plotted on log scale.

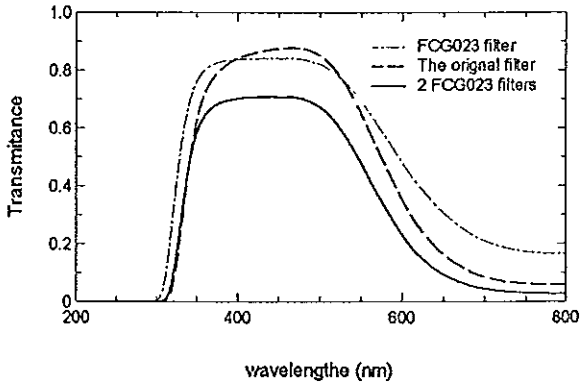


**Fig.4.4.** Transmittance of the different filters used to modify the white light spectrum

intensity compared with the red part. This results in a reduced signal to noise ratio, S/N, specially in the blue part of the spectrum. To improve the situation blue filters were used. Series of measurements were made using different blue filters to choose

the best filter available to the set up. Two FCG023 blue filters with the transmittance indicated in Fig. 4.4 were found to have less noise in the blue part when they were used in combination.

After the white light spectrum was measured the crystalline PIN detector was replaced by the colour sensor (NIPIN or 3-colour detector, 5-colour detector, or PIN detector). The colour sensors were a-Si:H thin films on glass substrate of 100cm² area with the TCO front contact and aluminium back contact. The area of one pixel of the sensor was 9mm². For connection of the sensor with the adjoining measuring circuit gold electrodes were used.

Unlike the crystalline photo detector used to measure the white light spectrum, the amorphous detectors work under bias in order to vary their spectral responses. Bias voltage was applied to the colour sensor using a set of dry cells and accumulators. Varying the bias voltage between 0V and +1V, and 0V and -3V for the 3-colour detector, between 0V and +3V, and 0V and -4V for 5-colour detector, and between 0V and -3V for PIN detector, the interferograms were taken and transformed into the corresponding spectra. The resulting spectra were recorded as intensity as a function of wavenumber.

In the procedure described above, the applied dc bias voltage resulted in a constant current which consequently resulted in the displacement of the signal (interferogram) up or down the screen. The displacement further amplified when the sensitivity of the amplifier was increased. This displacement puts a superficial limit to the maximum signal to noise ratio by moving the signal out of the monitor screen. To compensate for the displacement of the signal, the off set function of the amplifier was used. This is legitimate as the Fourier transform of a constant is a delta function at the origin, which lies out of the range of our interest. Thus, the displacement of the signal up or down by adding (or subtracting) a constant current would not affect the resulting measured spectrum.

Furthermore, the dc voltage supply and the voltmeter used to monitor the applied dc voltage were found to introduce high electrical noise signal. To avoid this the battery set was put in metal box and the voltmeter was detached each time after setting the voltage to the required values. The control of the movement of

mirror MM, the acquisition of the interferogram and the subsequent transformation to the spectrum were done by the computer with a program "PIEZ0".

### 4.2.2 Differential Spectral Responsivity

After measuring the spectral responses of the three kinds of a-Si:H thin film colour sensors with FTS, the measurements were repeated for the same pixel of each sample with the DSR equipment. This provides a reference data to compare with the data obtained from the FTS measurement. The set up shown in Fig. 3.1 was used with the exception that here the bias light was not used, as there is no need of attaining certain operating condition. Before starting the spectral response measurement the dark I-V measurement was carried out to make sure that the pixel was not damaged in transferring it from FTS set up to the DSR apparatus. This measurement was needed to avoid the risk of running the DSR apparatus with damaged sample, as the result with this device is to be obtained after a long time (after about one night for a sample). The rest of the measurement was as described in section 3.1.

# 5. Result And Discussion

## 5.1 Colour Separation and I-V Measurement

The measurement of the I-V characteristics of the three a-Si:H thin film colour sensor samples under constant monochromatic photon flux of $10^{15}$photons/cm$^2$/sec showed that the samples have reasonable ability of colour separation. the results of the measurement are shown in Fig.5.1(a) to (c). Different curves represent the I-V curves measured under different monochromatic light having different wavelengths.

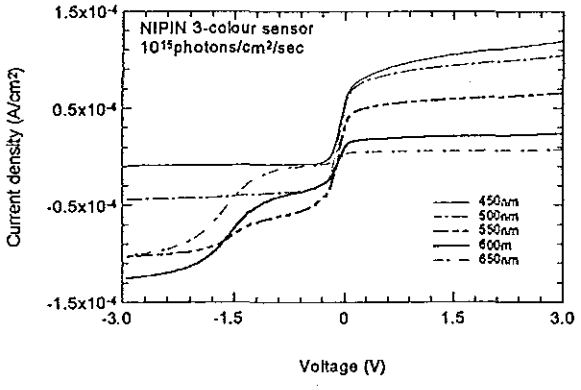


(a)

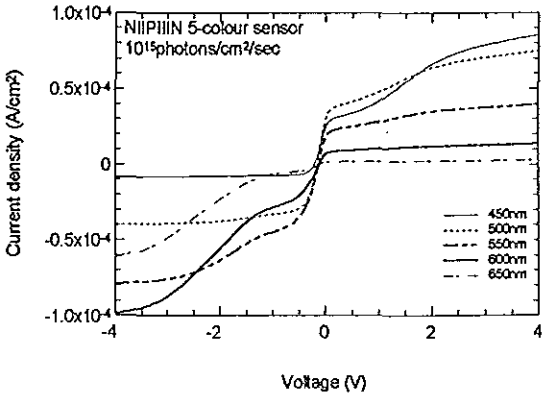


(b)

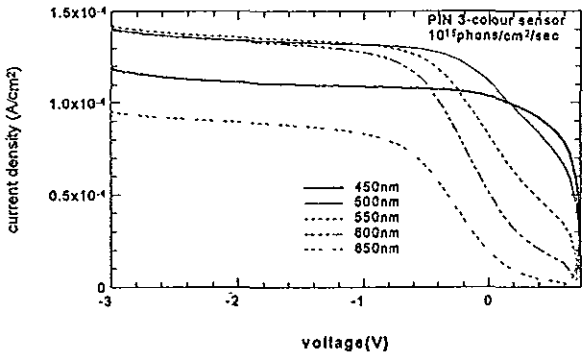


(c)

**Fig.5.1** The I-V curves measured under constant monochromatic photon flux with different wavelengths; (a) for three colour sensor, b) for multicolour sensor, and (c) for PIN sensor.

For the N-I-P-I-N three colour detector the photocurrent corresponding to the three primaries are dominant in different bias voltage ranges. For positive bias voltage the photocurrent corresponding to blue (450nm) monochromatic irradiance dominates over the others. In the range between 0V and about -1.7V the green (550nm) photocurrent is dominant. The photocurrent of the red photons (600nm) will have the largest magnitude in the range beyond -1.7V. One can also notice that in this range the contribution of photocurrent from the other components are

considerably large. This means, in the spectral response measurement the expected response will be the largest. A similar behaviour was observed also for the multi-colour sensor and the PIN detector.

## 5.2 The linearity of The Sensors

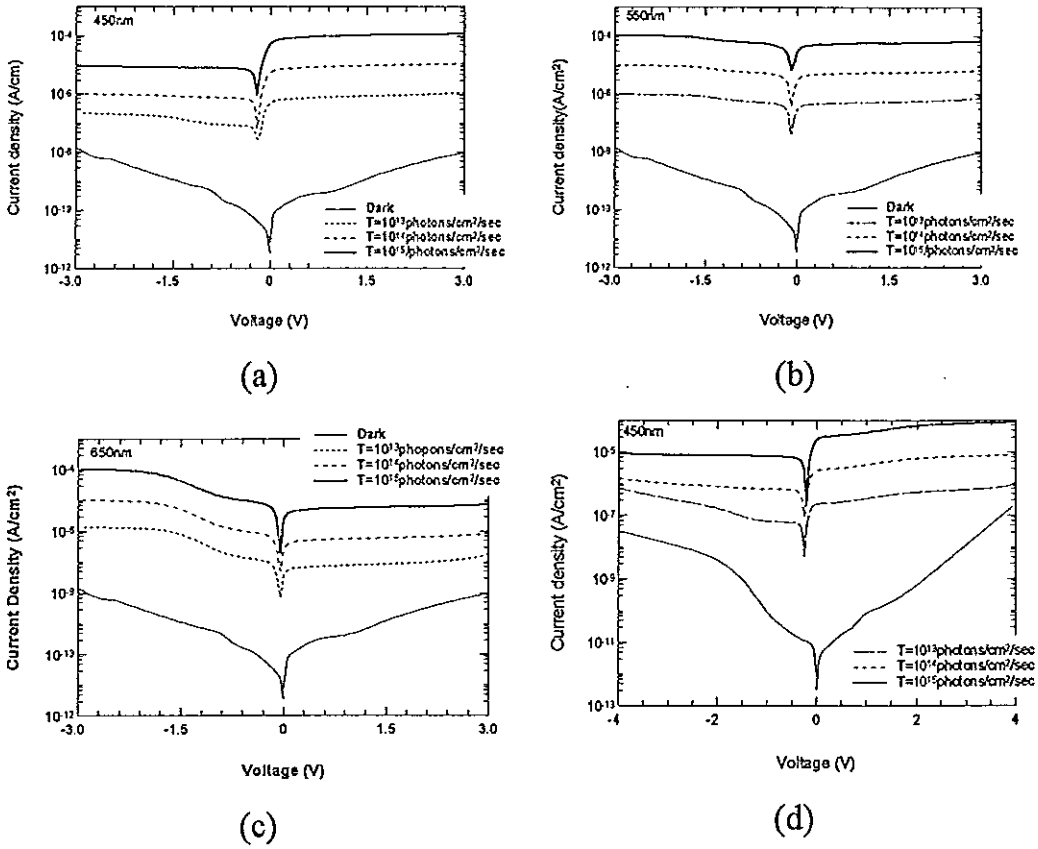


**Fig.5.2** Photocurrent of three colour detector under $10^{13}$, $10^{14}$ and $10^{15}$photons/cm$^2$/sec with (a) blue light, (b) green light, and (c) red light.
(d) The photocurrent for multi-colour sensor with blue monochromatic light.

From the measurements taken it was observed that the colour sensors have good linearity. In Fig.5.2(a) to (c) I-V curves showing the linear behaviour of the three colour sensor are presented. It can be seen that when the light intensity was increased by one order of magnitude, the resulting photocurrent increases also by the same amount. However, for small photon flux, the linearity seems to break at large bias voltages on the non-sensitive regions. This might happen due to large dark current which has comparable magnitude with the photocurrent. In Fig.5.2(d) the same deviation can be observed even with a larger correlation for the multi-colour sensor. This is because for multi-colour sensor larger bias voltage (as large

as 4V) results in larger dark current, and hence the observed diversion. The linearity test was carried out for the three samples with all the three colours. The observed behaviour was the same for all as described above.

## 5.3 The Dynamic Range

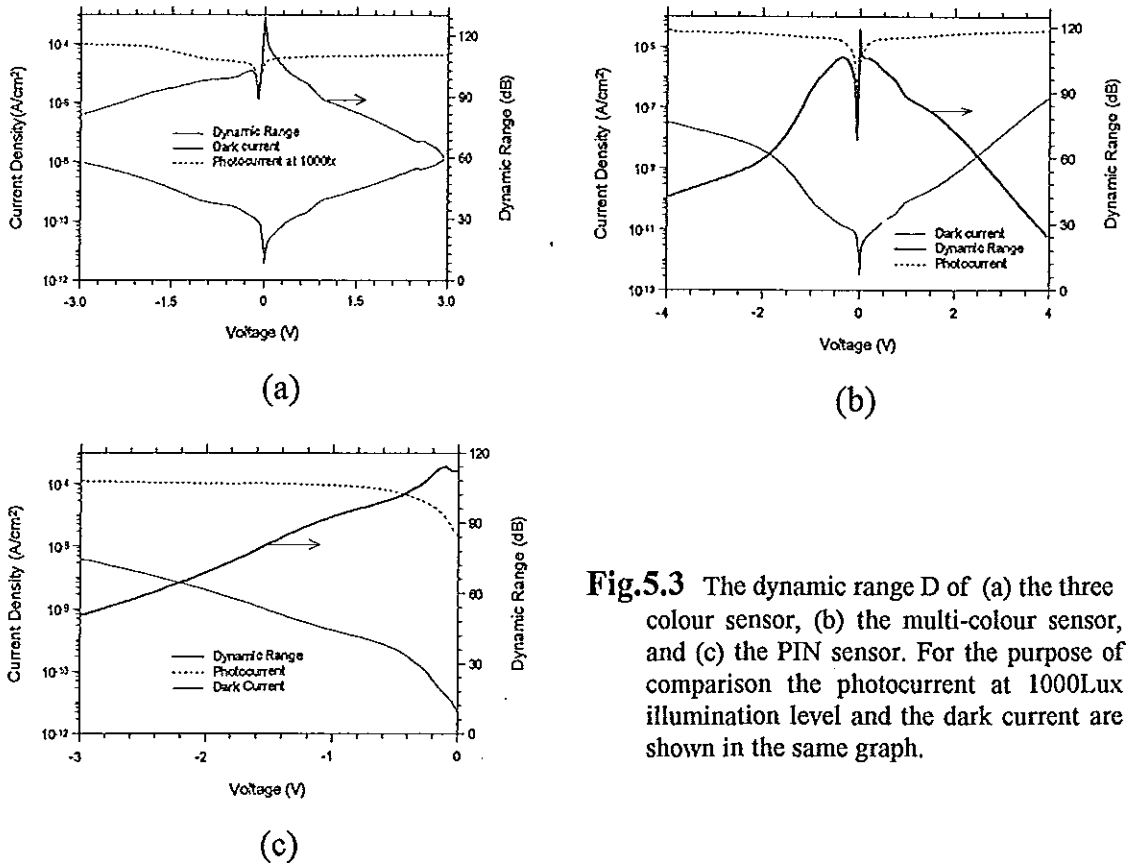


**Fig.5.3** The dynamic range D of (a) the three colour sensor, (b) the multi-colour sensor, and (c) the PIN sensor. For the purpose of comparison the photocurrent at 1000Lux illumination level and the dark current are shown in the same graph.

The dynamic range D is calculated taking the ratio of the photocurrent at illumination level of 1000Lux with a halogen lamp and the dark current. Even though the dynamic range falls to small values for large bias voltages, the samples exhibit good dynamic range at about the colour sensitive voltages. The relatively high dynamic range near zero bias voltage is due to a very small magnitude of the dark current. As discussed earlier in this paper the dynamic range strongly depends on the dark current in all the three cases. Specially, as the dark current of the multi-colour sensor and the P-I-N detector are large the dynamic range of these samples deteriorate to very small value rapidly. This might be improved by increasing the thickness of the a-Si:H film. Thicker film reduces the dark current, but, this will

negatively affect the response time of the device and it can also affect the colour separation.

## 5.4 The spectral response measurement results.

The measured Intensity distribution of the input white light $I_m(\lambda)$ can be given as

$$I_m(\lambda) = I_{in}(\lambda) S_c(\lambda) \qquad (5.1)$$

where $I_{in}(\lambda)$ is the actual input light intensity and $S_c(\lambda)$ is the multiplying factor characterising the measuring device. In this case $S_c(\lambda)$ is the spectral response of the crystalline silicon detector which was used to measure the spectrum. In determining the spectral response of the colour sensors, the input white light used to illuminate the sensors was $I_{in}(\lambda)$ which was measured at the beginning of each set of measurement as $I_m(\lambda)$. Hence, in calculating the spectral response it is $I_{in}(\lambda)$ which is needed rather than $I_m(\lambda)$. Thus the spectral response of the crystalline detector must be cancelled out from the acquired data by dividing $I_m(\lambda)$ through $S_c(\lambda)$ .

The crystalline silicon detector spectral response could be obtained from the manufacturer or can be measured. In this work it was measured by the SR measuring device. This response is shown in Fig.5.4. This curve was obtained from measurement of the response of the detector at each point separated by 10nm wavelength intervals. The white light spectrum $I_m(\lambda)$ is obtained in wave numbers which upon transformation gives $I_m(\lambda)$ as a function of wavelength in 1nm intervals. This difference in intervals causes difficulty in dividing two data of

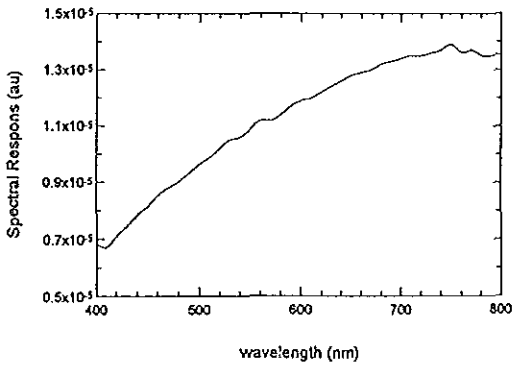


**Fig.5.4** The spectral response of the c-Si detector used for measuring white light spectrum.

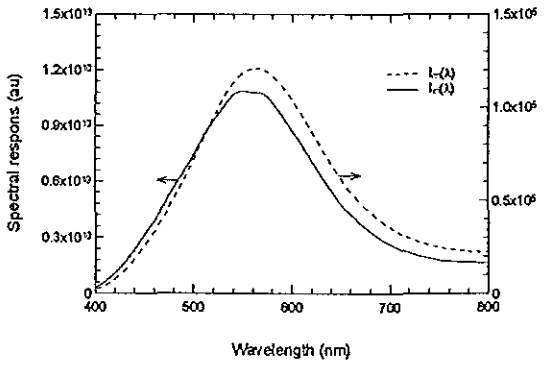


**Fig.5.5** White light spectra with and without correction for the influence of the spectral response of the c-Si detector on the measurement.

different bases through each other. For this reason the spectral response curve was splined (each intervals was divided into unit intervals and the corresponding values of $S_c(\lambda)$ for each interval was calculated or extrapolated from the original curve) by the computer program, "EASYPLOT".

After having both data in the same bases, the measured white light spectrum $I_m(\lambda)$ was divided by the spectral response $S_c(\lambda)$ of the crystalline detector. The resulting curve, $I_{in}(\lambda)$ was used in analysing the data to obtain the spectral response curves of the colour sensors. The spectral response curves were obtained by dividing the photo current $I(\lambda)$ measured with the a-Si:H detector by the white light spectrum $I_{in}(\lambda)$, i.e.,

$$S(\lambda) = \frac{I(\lambda)}{I_{in}(\lambda)} = \frac{I(\lambda)}{I_m(\lambda)/S_c(\lambda)} \qquad (5.2)$$

Fig.5.6 and 5.7 show the spectral response curves of the N-I-P-I-N colour sensor at different bias voltages. From Fig. 4.6 it can be noticed that for positive bias voltage, where the top diode is reverse biased, the spectral response curves peak at about 490nm. These curves are smooth and broad as there is non-zero probability of absorption (about 35%) of the green photons and red photons in i-layer of the top diode[30].

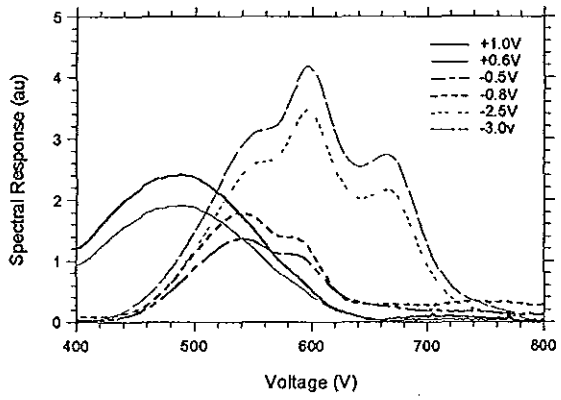


**Fig.5.6** The Spectral response curves of a three colour sensor at different bias voltages measured with FTS.

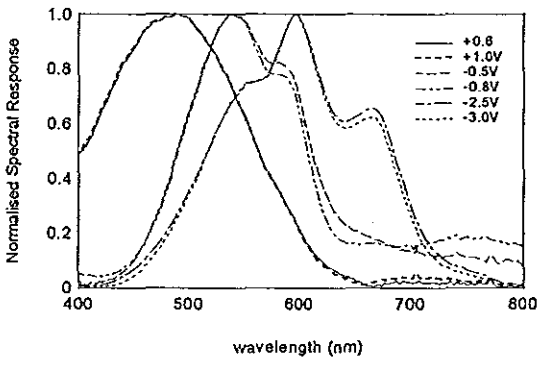


**Fig.5.7** The normalised spectral response curves of the thre colour sensor at different bias voltages. Here the separation between RGB signals can be seen.

When the bias changes in polarity, the photogenerated carriers collection region shifts to the bottom diode. For small negative bias voltages (<-1V) green photogenerated carriers from the i-layer close to the p-layer (See Fig.2.7.) are

collected. The spectral response curve, therefore, will have a peak in the green region. These curves show side plateau as the bias voltage gets larger (≈-1V). This is because of an increased probability of collection of carriers from the last i-layer. This side plateau progressively develops to a peak as the voltage is further increased. At about 2V and 3V a pronounced peak will be observed at about 600nm (red) in place of the plateau. For these bias voltages other two plateaus on either side of the peak will appear. One of them corresponds to the contribution of photocarriers in the first i-layer of the bottom diode. The other one, which will appear at about 650nm is due to interference effect.

The normalised spectral response curves give good insight into the colour separation. In Fig.5.5 the colour separation can be noticed. The peak spectral response of the sensor shifts from blue region (490nm) for positive voltages to green (540nm) for small negative voltages and to about 600nm (red) for large negative voltages. In the indicated ranges of bias voltages for different colour separations, increasing the bias voltage will not result in progressive shift of the maximum response. Increasing voltage results only in increasing the magnitude of the photo current as a result of improved collection of carriers. The shift is only a sudden one which results due to the change of the collection region of the photocarriers. This fact can be better seen from the normalised spectral response curves in Fig.5.7. The normalised curves were obtained by dividing the spectral response curves of Fig.5.6 by their respective maximum values.

The spectral response curves for the multi-colour detector are shown in Fig.5.8 and Fig.5.9. The same treatment applies to them as in the case of three colour detectors. Here too, colour separations, peak responsivities for different wavelengths at different bias voltages, are observed. For low positive voltages (V<1.0V) the top diode is reverse biased and the electrons in the rear i-layer of this diode are collected and the electrons and holes in the front i-layer are recombined effectively due to lower $\mu\tau$-product in this region. This gives peak spectral response at about 490nm. Increasing the bias voltage to higher value (~3V or less) moves the collection region into the front i-layer and hence a peak at 470nm. On the other hand for small negative voltages down to -1V range green light with a maximum at

530nm is detected. Increasing the magnitude of the bias to -2V shifts the maximum of the spectral response to 565nm because carriers generated in the middle i-layer of the bottom diode are collected. Further increase of the bias enables collection of the photogenerated carriers in the rear layer of the bottom diode. These carriers are generated by the red photons. This gives a maximum at about 585nm wavelength.

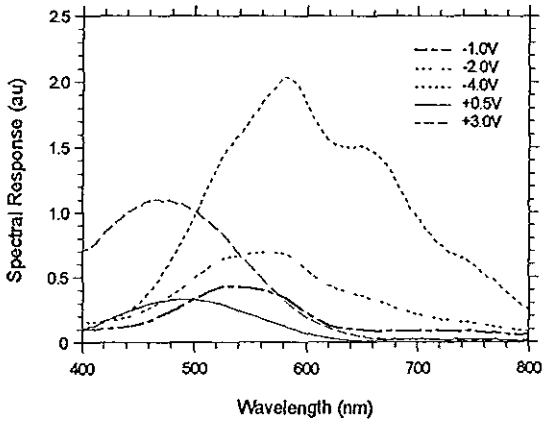


**Fig.5.8** Spectral response curves for the multi-colour detector. (FTS measurement)

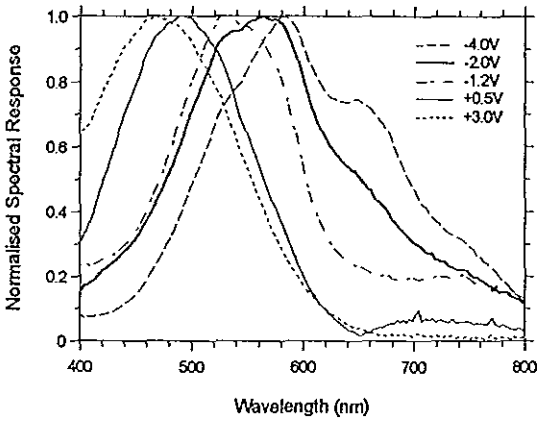


**Fig.5.9** Normalised spectral response of the multi-curves.

Similar measurements were taken for the P-I-N sensor. Representative curves measured with the FTS and the normalised spectral response curves obtained are presented in Fig.5.10 and Fig.5.11, respectively. In this sensor colour separation is possible for bias voltages less than -1V, at about -1V, and at about -2V. Change of the magnitude of the bias voltage results in the extension of the depletion region from

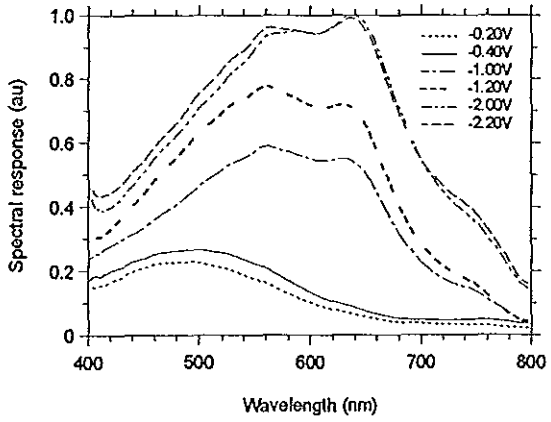


**Fig.5.10** Spectral response curves for the PIN colour sensor. (FTS measurement)

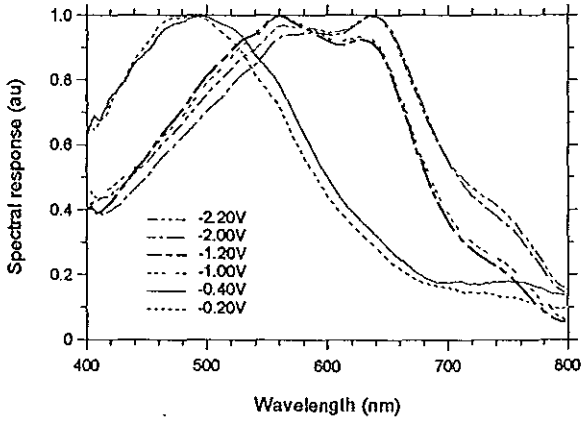


**Fig.5.11** Normalised spectral response of the PIN colour sensor.

the rear i-layer to the middle, then to the front i-layer. In Fig.5.10 the spectral response curves appear one below the other one. This is because as the collection region extends starting from the rear i-layer to the front i-layer carriers will be collected from the rear i-layer, the rear and the middle i-layers, and from all of the i-layers.

Essentially the same phenomena is observed when a spectral response set up with lock-in technique is used. The results of measurement with the SR apparatus are shown in Fig.5.12(a) to (c). These measurements were taken for the same samples and same pixels from each sample as used with FTS. For purpose of comparison representative curves from FTS and SR apparatus are plotted in Fig.5.13(a) to (c) for different colour sensors. As can be seen from these figures, the observed behaviours of the sensors are more or less the same. The shape of the spectral response curves look identical, and other features of the spectral responses, such as the plateaus are observed in both cases.

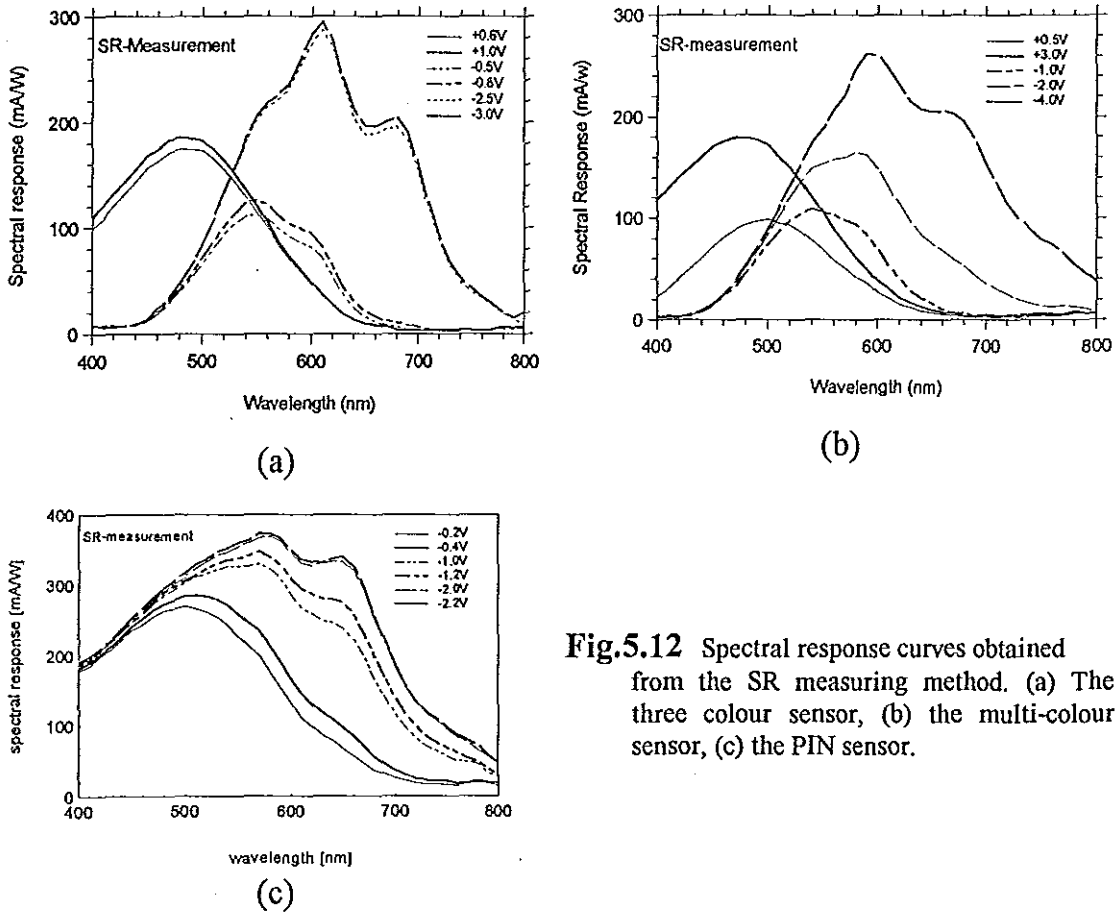


**Fig.5.12** Spectral response curves obtained from the SR measuring method. (a) The three colour sensor, (b) the multi-colour sensor, (c) the PIN sensor.

While there are many similarities between the data obtained with FTS and SR methods, there are marked differences between the two sets. The easily

recognisable difference is between the two sets of measurement data of the P-I-N sensor. In the case of the P-I-N sensor case the spectral response curves measured with the FTS are spread in the lower wavelength region while those of the SR are very close to each other. In addition to this, the side plateau on the higher

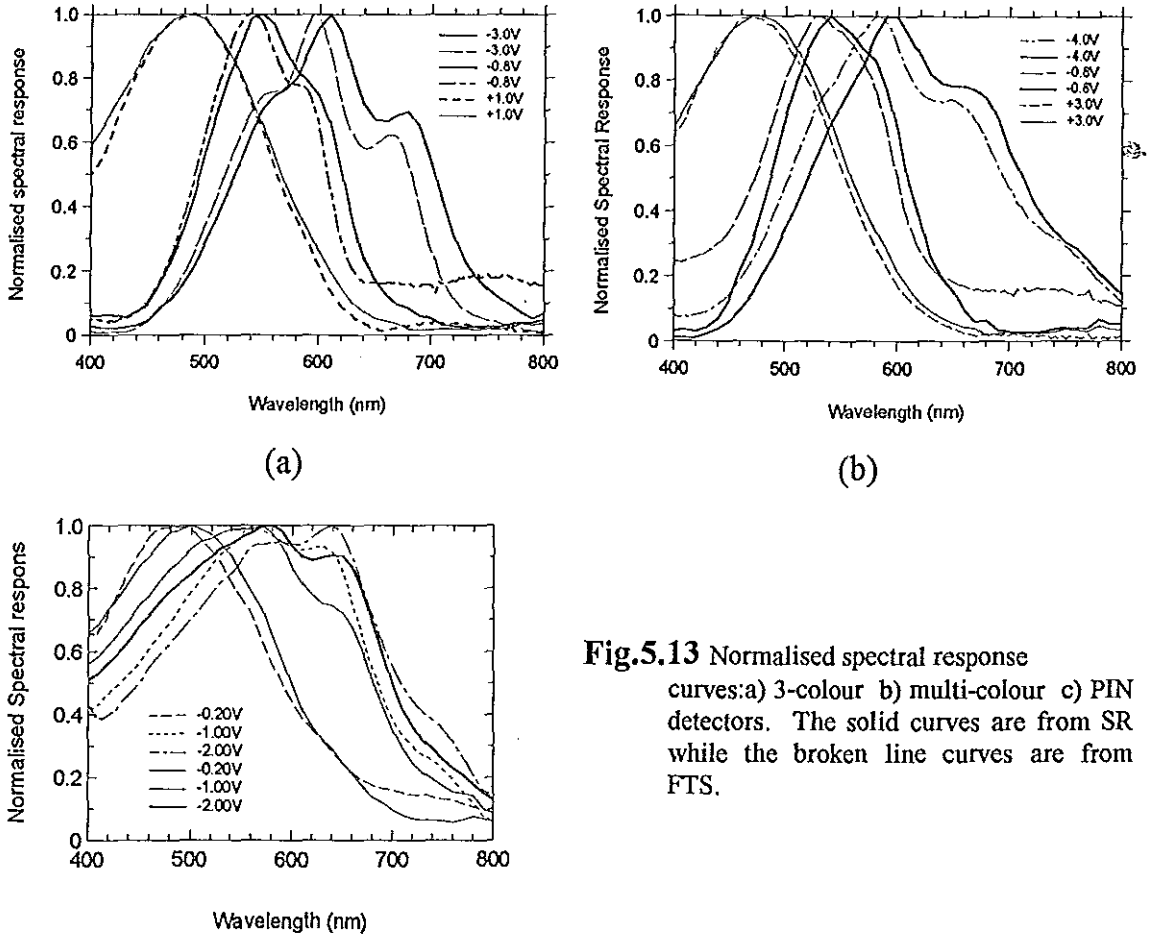


**Fig.5.13** Normalised spectral response curves:a) 3-colour b) multi-colour c) PIN detectors. The solid curves are from SR while the broken line curves are from FTS.

wavelength side already became a peak for about 2V in the FTS measurement. For all the samples the two sets of spectral response curves show difference as to the position of the maximum response. The difference is more apparent when the normalised spectral curves from the two set ups are plotted together. In general the spectral response curves measured with FTS are shifted towards the lower wavelength. The difference between the two sets of data increases as higher wavelength is approached. This difference is possibly caused by one or another or even by any combination of the following contributions.

a) The two measurement set ups are basically different. In principle it is possible for the two set ups to have inherently different accuracy due to differences in measurement principles. As noted earlier, no bias light was

used when the SR set up was used but for the FTS case there is always a constant bias light illuminating the sample. The effect of this bias light on the generation profile of the detectors is not known. However, we suspect a difference to emanate from these different measurement conditions. In addition to this the smallest units of the two measurements methods were not the same. While the data from FTS was in steps of 1nm, the SR data was in 10nm steps. This difference is believed to cause a shift of one set of data from the other set by about 5nm, to the maximum.

b) During calibration the part of the interferogram corresponding to the laser peak (633nm) is specified. But due to the unsteady movement of the piezo translator this particular point may not be exactly set. This was observed during the measurement process. As indicated in the procedure section, after calibration the laser peak was measured and it was observed to be found at different positions for different calibrations and different measurements. This situation can be illustrated using the laser peaks shown in Fig.5.14. These peaks were measured at different times for the one calibration case. It was not only the position of the peak that was observed to change, decreasing the peak and broadening of the spectrum were also observed. To the worst case this contribution may cause from 3 to 5nm shift.

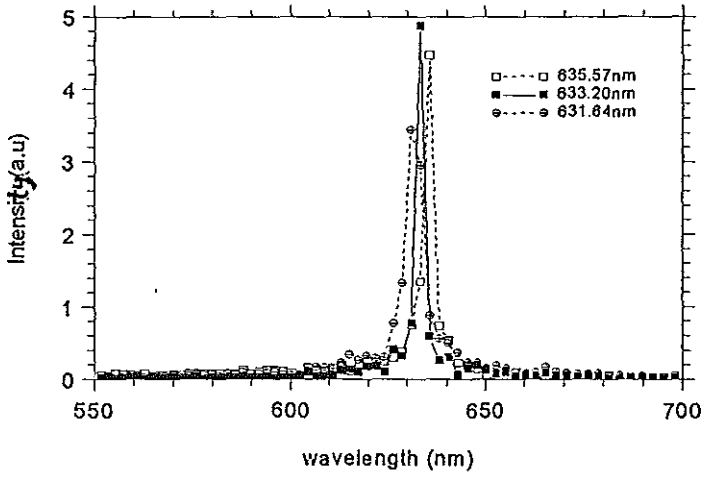


**Fig.5.14** Laser peaks measured with FTS at different times in otherwise the same conditions.

c) As the result of the combined contributions of the non-steady the piezo translator, the unsteady functioning of the powe halogen lamp and other unknown sources, the white light observed to vary in time. In Fig.5.15(a) two curves represe light spectrum and their ratio are shown. These two spectra v 15 minutes time difference between them in otherwise the sa To observe the effect of this shift of the white light spectrum response curve was arbitrarily chosen and it was multiplie curve. The resulting displacement of the peak obtained w One thing worth mentioning at this point is that the two curv Fig.5.15(b) are representing the worst case of the white l Hence, even if the white light spectrum is not temporally cons noticed that this variation has more strong influence on the response curve than on the position of its maximum.

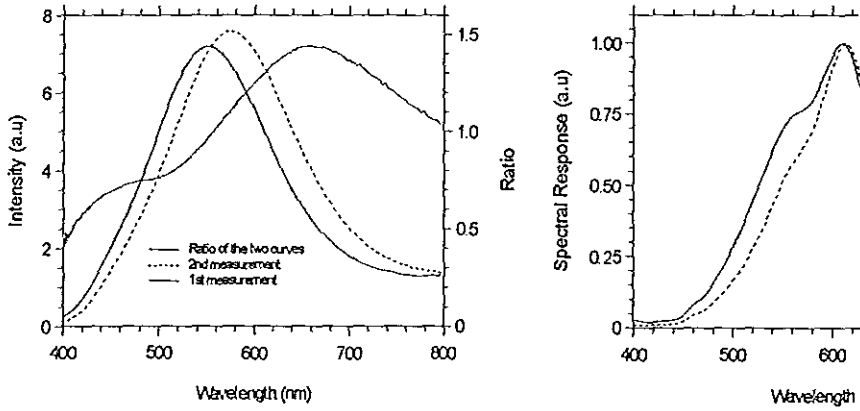


(a) (b)

**Fig.5.15** (a) Two white light spectrum curves obtained with a time diff between them. The heavy line is the ratio of the two. (b) A spectral respons product with the ratio of the two curves in Fig 5.15(a).

d) The other contribution identified is the systematic error of the used. To get a good signal to noise ratio, a preamplifie compensation was used. The compensation, however, introd which has the largest contribution of all. From measurement cut off filters and neutral filters, two competing effects were o

first is the intensity dependent one and the other is the sensitivity dependent one. These were obtained by determining the cut off wavelengths of different filters by reducing the intensity using neutral filters. This was

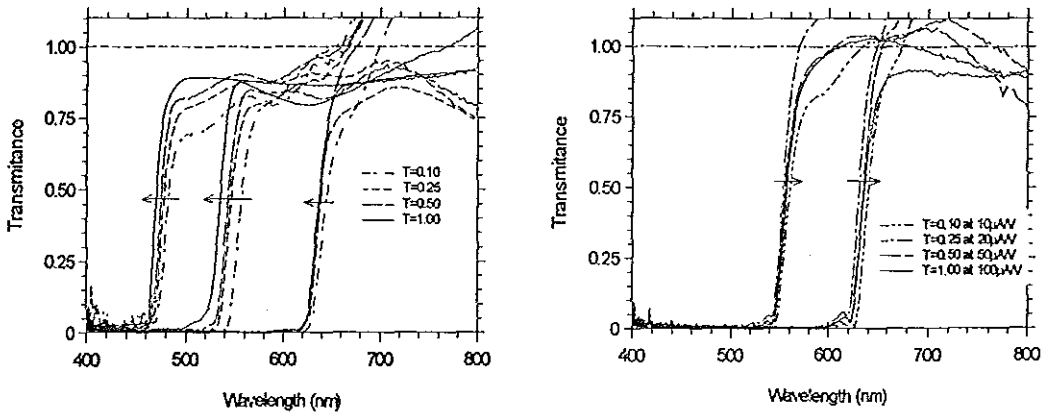


**Fig.5.16** Cut-off wavelengths for three different interference filters. (a) The measurements were taken by decreasing the intensity with neutral filters and making no compensation for it. (b) Cut off wavelengths for two different filters at different intensities and different preamplifier sensitivities.

done without compensating with the gain of the preamplifier for the former case and by compensating with the gain for the latter case. The results are shown in Fig.5.16(a) and Fig.5.16(b). As can be seen from these measurements increasing intensity results in a shift of about 10 or 15nm towards lower wavelengths. A decrease in sensitivity results in a shift of the same order but towards the higher wavelengths. This explains the shift towards higher wavelength in the blue part (where we have very low intensity) and towards lower wavelength in the red part.

# References


1. Zhu, Q et al, "A Novel a-Si(C):H Color Sensor Array," MRS Spring Meeting-Symposium A, San Fransisco, April 4-8,1994.
2. Stiebig, H et al, "Novel Multi-Spectral Detectors Based On a-Si:H Thin Film Technology," OPTO96 2nd Congress and Exhibition For Optical Sensor Technology Measuring Techniques Electronics, 1996.
3. Engelhardt, K & P. Seitz, Appl. Optics, Vol. 32, No. 16, 1763 (1993).
4. Frankie, Y, C.L. Eung & M.S. Demokan, Int. J.Opto., Vol. 9, No. 5, 367 (1997).
5. Tsai, H.K, S.C. Lee, & W.L. Lin, IEEE Electron Device Lett. EDL- 8, 365 (1987).
6. Tsai, H.K. & S.C. Lee, App. Phys. Lett. 52(4), 275 (1988).
7. Madan, A., "Utilization of Amorphous Silicon in Solar Cell Application," in Proc. 1st International Symposioum On Physic and Applications of Amorphous Semiconductors, F. Demichels (ed), World Scientific, Singapor, 65 (1987).
8. Cody G.D., "A Comparision of The Optical Absorption Edge of Crystalline and Amorphous Silicon," in Proc. 2nd International Symposioum On Physic and Applications of Amorphous Semiconductors, Toronto, 28 (1988).
9. Catalano, A., "Solar Cells Made of Amorphous And Microcrystalline Semiconductors," in Amorphous and Microcrystaline Semiconductor Devices: Optoelectronic Devices, J. Kanicki (ed), Artech House, Boston. 9-75 (1991).
10. Bohm, M. "Intelligent Image Sensor Systems in TRA (Thin Film on ASIC) University of Rookee, Roorkee U.P, India October 28-29, 1994.
11. Staebler D.L, & C.R. Wronski, Appl. Phys. Lett., Vol. 31, No. 4, 294 (1977).
12. Zhu, Q. et al, EUROPTO-Sensors and Control for Advanced Automation II, Frankfurt, Jun 20-24, (1994).
13. Bell, R.J., "Introductory Fourier Transform Spectroscopy", Academic Press, New Yourk, 1-77 (1972).
14. Beier. J., A. Schonecker, & A. Zastrow, "Spectral Response Measurements of Large Area Solar Cells With a Filter Monochromator System," 9th EPVSEC confference, Freiburg, Sept. 25-29, 394 (1989).
15. Bucher K. & A. Schonecker, "Spectral Response Measurements of Multi-Junction Solar Cells With A Grating Monochromator And A Fourier Spectrometer," 10th EPVSEC, Lisbon, April 8-12, 107 (1991).

16. Metzdorf, J., Appl. Optics, Vol.26, No.9, 1701 (1987).
17. Konopinski, E.J., "Electromagnetic Fields and Relativistic Particles", McGraw-Hill, New York, 181 (1981).
18. Levi, L., "Applied Optics: A Guide to Optical System Design" Vol.1, John Wiley & Sons, New York, 1-35 (1980).
19. Judo, D.B.and G. Wyszecki, "Colour in Business, Science and Industry", 3rd ed., John Wiley & Sons, New York, 40-90 (1975).
20. Nassau K., "The Physics and Chemistry of Color: The Fifteen causes of Color", Johon Wiley & Sons, New York, 15 (1983).
21. CIE Radiometric and Photometric Characteristics of Materials and Their Measurment, CIE Publ. No 28 (TC-2-3) Paris: Burean Central de la CIE.
22. Suzuki S., T. Kusunoki, and M. Mori, Appl. Optics, Vol.29, No.34, 5187 (1990).
23. Sze S.M., "Physics of Semiconductor Devices", 2nd Ed. John Wiley & Sons, New York, 743 (1981).
24. Jackson J.D., "Classical Electrodynamics", 2nd ed., John Wiley & Sons, New York, 298 (1975).
25. Shur, M., "Physics of Semiconductor Devices", Prentic Hall, Englewood Cliffs, N.J., 490 (1990).
26. Neamen, D.J., "Semiconductor Physics and Devices: Basic Principles", Irwin, Boston, 254 & 694 (1992).
27. Rose A. "Consepts in Photoconductivity and Allied Problems", Robert E. Krieger Pub., New York, 13 (1978).
28. Neidlinger ,T. et al, MRS symposioum Proc, (1996). to be Published.
29. Stiebig, H.et al, MRS Spring meeting San Francisco, 1996.
30. Eberhardt, K., T. Neidlinger, and M.B. Schubert, IEEE Transaction on Electron Device, Vol.42, No.10, 1763 (1995).
31. Stiebig, H. and M Bohm, J.Non-Crystalsine Solids, 164-166, 785 (1993).
32. Budde W., "Optical Radiation Measurements: Physical Detectors of Optical Radiation", Vol.4, Academic Press, Toronto, 36 (1983).
33. Topic, M. et al, MRS Symposium proc. 377., 779 (1995).
34. Metzdorf, J. et al, "The primary refference Solar Cell Calibration Facility at PTB", PTB, (1990).
35. Heidler, K. and B. Muller-Bierl, 10th EPVSEC, Lisbon, april 8-12, 111 (1991).
36. Manfred Zeider, "Ein Kompaktess Fourier Specktralphotometer fur das nahe

Infrarot und Sichtbare", Doctor of Ingeniering Dissertation, Aachemer Beitrage zur Physik der Kondensierten Materie, 1992.

37. Pain H.J., "The Physics of Vibrations and Waves", John Wiley & Sons, Singapore, 238 (1993).

38. Herres, H. and Gronholz, "Understanding FT-IR Data Processing", CAL Publication 4/84.

39. Morita K., "Applied Fourier Transform", Ohmsha-IOS press, Tokyo, 33 (1995).